Review

Literature Review on Thermomechanical Modelling and Analysis of Residual Stress Effects in Wire Arc Additive Manufacturing

Fakada Dabalo Gurmesa * and Hirpa Gelgele Lemu *

Department of Mechanical and Structural Engineering and Materials Science, Faculty of Science and Technology, University of Stavanger, N-4036 Stavanger, Norway
* Correspondence: ff.dabalo@gmail.com (F.D.G.); hirpa.g.lemu@uis.no (H.G.L.); Tel.: +47-46366532 (F.D.G.); +47-51832173 (H.G.L.)

Abstract: The wire arc additive manufacturing (WAAM) process is a 3D metal-printing technique that builds components by depositing beads of molten metal wire pool in a layer-by-layer style. Even though manufactured parts commonly suffer from defects, the search to minimize defects in the product is a continuing process, for instance, using modeling techniques. In areas where thermal energy is involved, thermomechanical modeling is one of the methods used to determine the input thermal load and its effect on the products. In the WAAM fabrication process, the thermal load is the most significant cause of residual stress due to the extension and shrinkage of the molten pool. This review article explores the thermomechanical effect and stress existing in WAAM-fabricated parts due to the thermal cycles and other parameters in the process. It focuses on thermomechanical modeling and analysis of residual stress, which has interdependence with the thermal cycle, mechanical response, and residual stress in the process during printing. This review also explores some methods for measuring and minimizing the residual stress during and after the printing process. Residual stress and distortion associated with many input and process parameters that are in complement to thermal cycles in the process are discussed. This review study concludes that the thermal dependency of material characterization and process integration for WAAM to produce structurally sound and defect-free parts remain central issues for future research.

Keywords: wire arc additive manufacturing; thermomechanical modeling; thermal residual stresses; residual stress; distortions

1. Introduction

Wire arc additive manufacturing (WAAM) is a type of additive manufacturing (AM) process that uses an electric arc welding technique with a wire feeding process and provides a high deposition rate [1–3]. Previous investigations showed that the method is carried out using a layer-by-layer approach to build the part, and the corresponding heat input influences the mechanical properties of WAAM products [4]. Understanding the thermal history of thermomechanical and thermal gradients in the WAAM process leads to the possibility to determine common product defects such as residual stresses (RS), distortion, and microstructure defects in WAAM products. It provides a description of those factors in the WAAM process that influence the characteristics of the formation of the molten pool and bead geometry. The RS and distortion are partly caused by the effects of preventing ionization as a result of the nearby low temperature and a contracting orifice in its inner wall [5–9]. Furthermore, components manufactured by WAAM are mostly affected by RS because of the high heat input from the electric arc source induced between the workpiece and wire, which is the cause of the overall mechanical response [10–13]. As a consequence of thermal complexity in the process of WAAM, the RS induced is also considerably complicated [14]. Particularly, the effects of thermal complexity behavior in fabrication show a significant role in the mechanical behaviors and geometrical formation of components manufactured with WAAM technology [15].

Wire-feed AM processes in general contain high remaining stresses and distortions because of excessive heat input and an excessive deposition rate [16]. Similarly, in wire-feed AM technology, the energy input, welding speed, wire diameter, wire-feed rate, deposition sequences, and deposition pattern, etc. are factors of RS on the thermal history of the process. In addition to their effects on defects, the above-listed factors also affect the surface roughness and accuracy of the products. Specifically, the influence of heat accumulation on the arc stability, bead formation, and metal-transfer behavior during the printing process need to be given attention during the printing process [17–22]. Furthermore, monitoring or determining the interlayer temperature (IT) is one of the significant measures to enhance WAAM product quality. In the case of mitigation of part distortion, compressed CO_2 is actively used in the interpass cooling. The temperature in the building rises as the thermal mass increases with energy input. To track thermal gradients and ensure proper thermal management, non-contact thermal monitoring, that is, thermal imaging, can be used [23,24]. Heat input accumulation during layer deposition causes high RS in WAAM components. The results of RS developed in the products are defects such as delamination, cracks, distortion, and low fatigue life [25].

The metallographic and mechanical characteristics of parts manufactured by WAAM using gas metal arc welding (GMAW) and plasma arc welding (PAW) indicated that PAW is slightly increased in elongation and toughness compared to GMAW [26], which could be due to the difference in the thermal input. The concept of welding simulation is very supportive for both WAAM and the welding process because, in both cases, metals are melted to build the parts. Due to the thermal cycle in the melting process, RS and distortion lead to non-uniform contraction and expansion mechanisms in the materials [27]. Figure 1 [28] illustrates the region where the melting front in the WAAM process is heated up sharply and lets the material fuse locally during the process of deposition, in a similar fashion as the arc welding process [29].
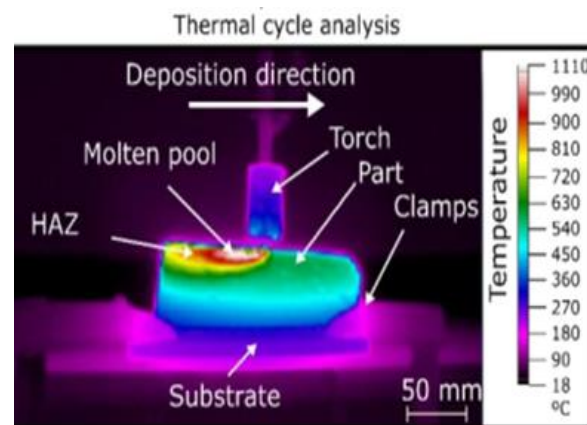

Figure 1. Thermal cycle analysis of the WAAM process (Reprinted with permission from ref. [28]. Copyright 2019 Elsevier, License Number-5462710771792).

The objective of this review article is to explore the thermomechanical modeling and RS effects of the WAAM process. Following this introduction section, the article is structured as follows: Section 2 presents the methods used to review the articles and the statistics of the cited articles with publication year, followed by an analysis of the thermomechanical modeling approaches of the WAAM process and the residual stresses caused by thermal and mechanical effects in Sections 3 and 4, respectively. Then, Section 5 deals with the discussion of a useful outlook, and finally, the conclusion is drawn in Section 6.

2. Materials and Methods

To address the objective of the article, this literature review focuses on the most recent articles (whose statistics are displayed in Figure 2), except for some exceptions, and the

content is thematically organized with topics or issues. The search was limited to sources that have published articles in English only. The databases used in this review include Google Scholar, elibrary.ru, Free Full PDF, INGENTA, Polish Scientific Journals, Database, Science Direct, Springer Nature, Worldwide Science, WorldCat, Open Access Journals, IOP, JST, WS, ISSN, and peer-reviewed journals.
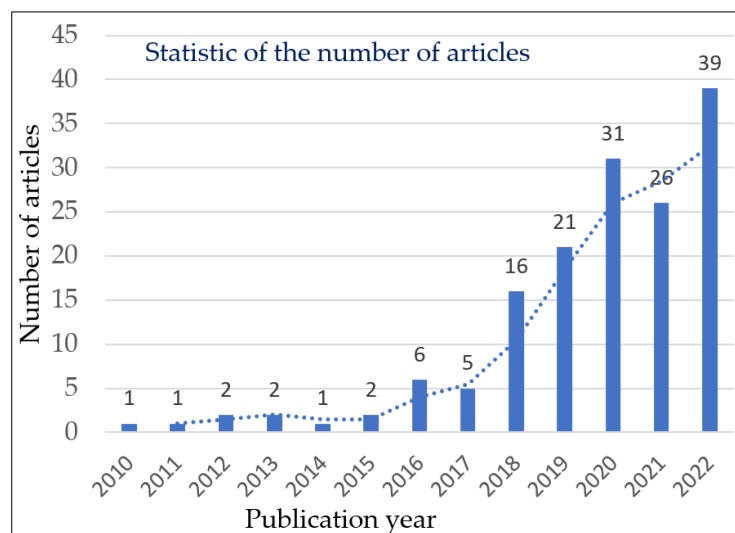
Figure 2. Statistics of reviewed articles on the WAAM process.

Though this review work may not cover all possible relevant works worldwide, it has reported research results reported in 152 articles to put together recent progress in thermomechanical modeling and analysis of residual stresses in WAAM. As displayed in Figure 2, the largest number of articles reviewed for this work are those reported in 2022.

3. Thermomechanical Modeling of the WAAM Process

Thermomechanical modeling provides the description, methodology, and backgrounds of WAAM techniques to assist the production process and increase the quality of printed parts based on the concepts of thermal and mechanical analysis. Though most recent research on WAAM focused on modeling techniques, many studies merged both modeling and experimental works for the sake of validation. For instance, Ding et al. [30] studied both the mechanical and thermal models with the finite element (FE) software package ABAQUS 6.10 using Eulerian and Lagrangian reference frames for a steady state and a transient thermal model, respectively, and validated them with experiments. The study also indicated that, in the WAAM, the higher power input of the welding process causes major RS and distortion of the manufactured components. Cambon et al. [31] conducted experimental work on the thermomechanical model to separately explain the heat effect in the WAAM process and on a mechanical model to study the expansion and the solidification leading to shrinkage. The mechanical properties of parts produced using WAAM are affected by the thermal residual stresses when the stress results exceed the local yield stresses and experience plastic deformation [32]. Other researchers, such as Li et al. [14], conducted a coupled thermaomechanical model to determine the thermal stresses and the distributions of RS using a GMA-based AM process in the MSC. Marc code. The hole-drilling method was used to measure the RS generated in the deposited layers and substrate to confirm the effectiveness of the model.

For the entire WAAM process, the thermal properties of solids and liquids such as the thermal conductivity, density, specific heat, emissivity, and latent heat are used for melting the wire. Similarly, the mechanical properties such as the yield strength, elastic modulus, and thermal expansion coefficient, as well as the elastic and plastic strain of the materials

that are functions of temperature are used during the process to predict the expansion and contraction of molten beads, as reported in the literature [33,34].

Numerical simulation is the best way to represent the thermal phenomena existing in WAAM during the process. Among others, the finite element method (FEM) is used to model the deposition of material and heat input during the WAAM process [35]. For instance, Tangestani et al. [36] studied the process for enhancing the mechanical properties using both thermomechanical FEM and experimental tests, in which the results revealed that the profile of RS in the pinch rolling process is sensitive to the direction of rolling. It was also observed that more compressive RS could be made into the wall by applying fewer passes of rolling with thicker rollers. As reported in [14,37] the distributions of RS in the parts along the deposition pathway on the inside surfaces and on the outside of the fifth layer are equal to zero transversal RS. In the WAAM process, 3D thermomechanical transient simulation within FEM can give comprehensive and correct temperature distribution predictions, the distortion and stress distribution, as well as the thermal history of built parts. All temperature-dependent thermal properties are required to accurately simulate the process from solidus to liquidus transition and the heat-affected zone [1,38].

3.1. Thermal Modeling

Thermal modeling in the WAAM process is important to specify an optimum process parameter with geometrical consistency for the desired production by moderating the heat inputs. RS and distortions are considered to be the major obstacles against the more widespread application of WAAM. In particular, since WAAM involves significant amounts of heat input within the printed part, thermal management is the main important action needed to improve the quality of the part in cases of surface finish and induced internal voids [39,40]. For these defects, thermal modeling can provide the basis for the thermal properties of the RS remaining in the products. As the moving localized heat source causes steep temperature gradients, which are inevitable in this process, accurate prediction of the thermally induced RS and distortions is of paramount importance. The properties of the thermally affected build-up part are due to the layer-by-layer molten pool deposits and process conditions such as the deposition patterns, energy input, and heat conduction during the printing process [18,41].

Wire and arc-directed energy deposition (WADED) is among the metallic AM technologies that are most important in monitoring the temperature evolution since it directly affects the deposited quality of parts. The history of temperature in WADED can be attained using numerical simulations and/or experiments [42]. The thermal cycle in the WAAM was applied equally as a thermal load for each bead according to the welding process. The heat source parameters gained as a result are used for carrying out thermal and mechanical analysis. The influence of the heat input on the grain size, tensile properties, hardness, and impact toughness along the building direction are studied [29,43], which reveal superior tensile properties and hardness. However, variation in the mechanical properties are due to grain sizes and microstructural evolution evolved with the level of heat input. The heat input of the WAAM process arc melts the wire into the molten pool to make the parts. The heat loss modes in such processes are discussed and illustrated in several studies, such as [20,44,45]. The adjacent tool-path concentration makes fragments in the thermomechanical properties of continuous tool-paths that are likely to be poor, bringing about a degradation of performance and other defects [46].

Based on the heat input parameters, mathematical modeling [47,48] and management concepts are related to RS, tension, shrinkage, and deformation, which are critical and particularly covered in [49,50]. In such mathematical modeling works, a general equation of energy balance based on the First Law of Thermodynamics is often used, which is given in Equation (1):

$$Q_L = Q_C + Q_{C_v} + Q_R \tag{1}$$

where Q_L is the quantity of heat loss, Q_C is the conduction loss, Q_{C_v} is the convection loss and Q_R is the radiation loss. The heat losses by radiation and convection from the surfaces

of the substrate and deposit are applied as boundary conditions [9]. As reported in [10,51], the transient temperature fields over the part geometry in all directions were calculated from the 3D heat conduction equation, which is given in Equation (2). In this formulation, the thermal model was sequentially coupled to the mechanical model. Regarding the heat source model in the AM process, the heat transfer equation of the arc in the material and transient temperature fields is given by the Fourier equation for a transient and non-linear system, which is the heat-conduction equation during the process of deposition [10,14,51], as shown in Equation (2).

$$\lambda\left(\frac{\partial^2 T}{\partial x^2}\right) + \lambda\left(\frac{\partial^2 T}{\partial y^2}\right) + \lambda + q_v = \rho c\left(\frac{\partial T}{\partial t}\right) \tag{2}$$

where T is the temperature, λ is the material's thermal conductivity, q_v is the heat source or sink, ρ is the material density, c is the specific heat capacity of the materials, t is the time of heat transfer, and x, y, and z are coordinates in the space coordinate system.

The heat source model of a dual ellipsoid was used to simulate the heat input in the AM process [52] as shown in Figure 3a. The movement of the heat source simulation and the temperature change position are also shown in Figure 3b [11].

(a) (b)
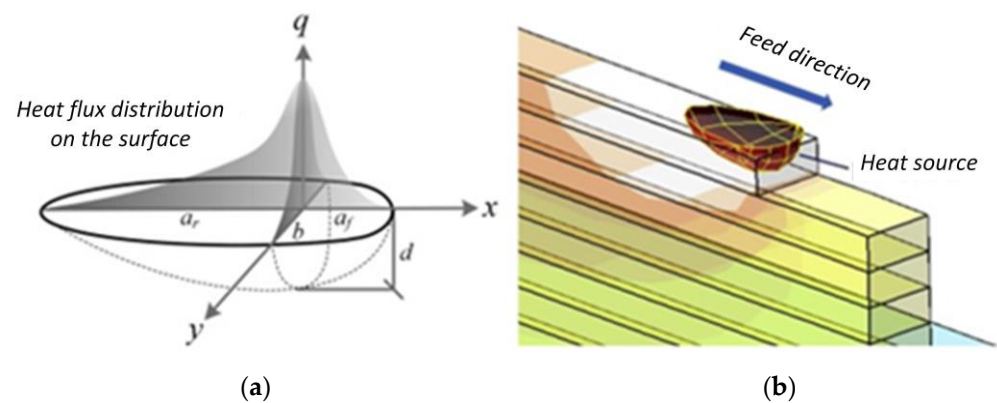
Figure 3. Illustration of (**a**) parameters of heat source volume with double ellipsoidal shape and (**b**) heat source movements and activation approach of mesh elements in the simulations (Reprinted from ref. [11]. Copyright 2019, Elsevier, in accordance with CC BY license, open access).

The front and rear halves of the heat flux densities are further discussed in the relevant literature [30,53–55], and the formulas are presented in Equations (3) and (4), respectively.

$$q_f(x,y,z) = \frac{6\sqrt{3}f_f Q}{\pi a_f bc\sqrt{\pi}} exp\left[-3\left(\frac{x^2}{a_f^2} + \frac{y^2}{b^2} + \frac{z^2}{c^2}\right)\right] \tag{3}$$

$$q_r(x,y,z) = \frac{6\sqrt{3}f_r Q}{\pi a_r bc\sqrt{\pi}} exp\left[-3\left(\frac{x^2}{a_r^2} + \frac{y^2}{b^2} + \frac{z^2}{c^2}\right)\right] \tag{4}$$

$$f_f + f_r = 2$$

where a_f and a_r are the lengths of the frontal ellipsoid and rear ellipsoid, respectively; b is the heat source width; c is the depth of the heat source, which is the heat source parameter; Q is the efficiency factor of energy input; and f_r and f_f are the distributing power factors for the rear and front heat source, respectively. The high-density electron beam heat source was modeled as a conical volumetric heat source with a Gaussian distribution or double

ellipsoid volumetric heat source model, as given in Equation (5). The intensity distribution profile can be adopted and modified from the mathematical modeling [10,33].

$$Q = \frac{2}{h}\left(1 - \frac{z}{h}\right)\frac{3 \times \eta \times V_a \times I_b}{\pi \times \varnothing_e^2}exp\left(-\frac{2(x^2 + y^2)}{\varnothing_e^2}\right) \tag{5}$$

where Q is the power generated per unit volume, h is the penetration depth, η is the heat source efficiency, V_a is the accelerating voltage, I_b is the beam current, $\varnothing_e$ is the beam diameter, and x, y, and z are the local coordinates of a point on the part geometry.

Convective heat losses on the surface caused by the forced mechanism are ignored since the EBAM process is carried out in a vacuum. Radiation heat losses were considered from all outer free surfaces according to the Stefan–Boltzmann law as shown in Equation (6):

$$q_{rad} = \varepsilon\sigma\left(T_{srf}^4 - T_\infty^4\right) \tag{6}$$

where ε is the emissivity, σ is the Stefan–Boltzmann constant, T_{srf} is the surface temperature of the part, and T_∞ is the ambient temperature (298 K).

Wu et al. [56] investigated the arc stability, bead formation, and metal transfer mechanisms during the fabrication of Ti6Al4V. From heat accumulation by gas tungsten WAAM, the effects of localized gas shielding and heat accumulation indicate the deposition constancy during the WAAM process control and component optimization. Others studied the indication of comprehensive thermal characteristics of a WAAM process and pointed out the thermal effects on the geometrical accuracy, process stability, and deposited part properties. The deposited beads' temperature profile and the solidification parameters are examined using experimental and numerical simulation models that reflect the deposition process characteristics [22,57–59]. Inconsistent layer cross-sectional dimensions and undulated surface appearance are two types of defects observed in WAAM products. These are due to an inadequate heat input and nonlinear time-varying boundary conditions of the thermal effect in the molten pool [60]. Fluid flow and heat transfer models are usable to join process variables and parameters that affect the properties of printed parts. Both the arc pressure and the convective flow are the two main factors that govern the depth and width of penetration, respectively [61].

The summary of arc welding types and thermal distribution effects on the WAAM components is given in Table 1.

Table 1. Some reviewed effects of thermal distribution on the specific study in the WAAM process.

Arc Welding	Focus Area	Specific Area of the Study	Citation (Year)
EBM	Microstructure, macrostructure, and mechanical properties	Effect of heat input in WAAM process	[62] (2021)
GMAW	Geometric accuracy, productivity, and microstructure	Geometry regulation of thermoelectric cooling-aided bead in WAAM of thin-walled structures	[63] (2018)
CMT and C-GMAW mode	Microstructure transformations and mechanical properties	Thermal effect on evolution of microstructure and mechanical properties in WAAM components	[64] (2022)
GT-WAAM	Influences of heat accumulation, surface oxidation, and bead geometries in building direction	Heat accumulation effects on the arc characteristics and metal transfer behavior in WAAM	[56] (2017)
GMA-AM	Multi-track depositions for different processing conditions for defect formation	Improving fluid flow and heat transfer model of WAAM	[61] (2021)
GT-WAAM	Heat accumulation effect on microstructure and mechanical properties of AM products	Heat impact on microstructure deposited and mechanical properties by WAAM	[15] (2018)
GMAW and PAW	Analysis of wall geometry, metallography, and mechanical properties.	Heat input effect on WAAM of Invar: microstructure and mechanical properties	[26] (2022)
GMAW-CMT	Assumption of thermomechanical analysis	Method of computing temperature and RS in WAAM component	[31] (2020)

A high-temperature gradient near the melt pool leads to undesirable product dimensional distortion and deformation, which is the outcome of rapid thermal cycling. When the product is exposed to excessive strain due to thermal strain, it is more susceptible to fracture, which decreases the component life expectancy and increases the risk of early component failure [18]. The direction of deposition influences the residual strain and stress during the welding process of a single-pass multilayer [29,65]. The physical properties of the components made using WAAM depend on heat input during the printing process [48]. Similarly, physical properties such as the thermal conductivity and specific heat conductivity were increased with temperature while the density, viscosity, Young's modulus, and yield strength decrease with increased temperature [66]. Moreover, thermomechanical simulation to predict the thermal flow and numerical analysis for metal addition during the deposition process are performed. The numerical analysis is validated with experimental investigation results by considering the effects of welding parameters such as the arc current, arc voltage, wire speed, welding speed, wire diameter, shielding gas, heat sources, and temperature fields, as studied and reported in [17,31,67].

In [51,68], it has been reported that a thin substrate and low interpass temperature are capable of minimizing the tensile RS in the WAAM products. The study also indicated that mechanical properties and microstructural characteristics are strongly dependent on the thermal history during printing. Likewise, significant temperature gradients, high heating and cooling rates, bulk temperature rises, and periodic thermal cycles cause variation in printed parts' properties. One of the key factors in the WAAM process is thermal management to mitigate the accumulation of heat and cope with restrictions concerning geometry issues, the deposition cycle, and anisotropies in the mechanical properties [69,70]. Furthermore, a theoretical model was developed to optimize the heat input and the interlayer temperature for the deposition of each layer. In thin-walled structures built up in the WAAM process, molten pool solidification and bead geometry vary as wall height increases, mainly due to heat dissipation on the substrate. An active cooling system during the process using the technology of thermoelectric cooling is used to eliminate the variance in the dissipation of heat between the lower and upper layers [24,31,63]. The evolution of microstructure in the WAAM process depends on the material's thermal history, which is estimated using FE modeling. Transformations of the microstructure are assessed with a diagram of continuous cooling transformation, and the microstructure is investigated with the use of scanning electron and optical microscopy. Similarly, the impact of temperature interpass on the hardness and microstructure was studied in [64,68,71] for AM80 HSLA steel, and the result revealed that a high interpass temperature leads to the development of martensite. During the WAAM process, heat accumulation results in the deposition of a multi-layer increase in the temperature preheat in the preceding built layer. These reasons lead to instabilities in the interlayer density, microstructure, mechanical properties, and geometry, which evolve differences in the material properties [72,73]. There are two types of temperature-measuring methods in the WAAM process: (1) contact (thermocouple) [10,30,33,74] and (2) non-contact measuring (infrared camera, pyrometrical methods, etc.,) [27,39,75,76].

3.2. Mechanical Modeling

Since the WAAM process has different thermal effects leading to varying mechanical properties of the printed parts, the process is examined in different building directions, which gave different results [18]. Additionally, variation in the substrate geometry has a significant effect on the molten pool geometry and heat transfer condition, which influence the welding for deposition of the WAAM process [1,77]. However, mechanical analysis to evaluate the stresses developed in the WAAM-printed products is carried out with a thermal load employed in finite element analysis (FEA) that caused RS and distortion. No significant variances were realized in either the mechanical or microstructural character succeeding heat treatments in air, in a vacuum, or in argon [78–81]. In the mechanical

analysis, the clamping conditions (i.e., degrees of freedom constraints) have an important influence on the printed products [72].

The Lagrangian thermal model and nodal temperature results from the thermal analysis are used as thermal load inputs for the mechanical analysis [30,82]. Another investigation was performed in [30] using the Eulerian thermal model to calculate the steady-state temperature distributions, which are used as inputs to a 3D mechanical model for RS and distortion analysis. From the results of both the experimental and numerical studies, the temperature, distortion, and RS were compared and showed good agreement. Chen et al. [83] conducted a study of the superalloy (Ni-17Mo-7Cr) component fabricated with WAAM. The results showed stability in both tensile and hardness properties while a sharp reduction was perceived in the layers of the superficial surface. Thermal evolution is coupled to an elastoplastic mechanical boundary condition value problem that calculates the thermal stresses and distortions with Goldak thermal modeling approach. It was extensively modeled for accuracy by comparing the mechanical properties and thermal predictions with the equivalent experimental measurements with a non-linear transient function [41,53]. Hejripour et al. [84] studied on two parts built with WAAM, i.e., (1) wall and (2) tube from 2209 Duplex Stainless Steel. The results indicated that the slow rate of cooling for layers built at high temperatures caused austenite creation significantly in a ferrite matrix. The correlation between the developed thermal model for phase transformation and cooling rates is quite accurate to predict thermal cycles and weld zone profiles [7,69,85,86].

Even though WAAM technology is an energy-efficient manufacturing method for metal production, heat accumulation during deposition and associated mechanical changes result in RS, which was observed in the profiles across the cross-section of the printed components [25,87]. The mechanism of crack formation in a WAAM-manufactured Al-Zn-Mg-Cu alloy, which has high crack sensitivity, was studied using a combination of microstructure analysis and thermal-stress simulation [65,67]. The results indicated that increasing the deposition height increases the stress, which leads to crack propagation and the appearance of a macrocrack. In other studies, it has been reported that WAAM-manufactured super duplex stainless steel has both excellent corrosion resistance and mechanical properties [67,88]. In the studies, the microstructure of the wall deposited was carefully examined for variation in the mechanical properties. The results also revealed that the austenite/ferrite balance of phases in the wall body was fragmented by the overgrowing of the austenite phase. The anisotropic examination revealed that the ultimate tensile stress (UTS) and elongation appeared separately in the horizontal and vertical directions. The yield stress (YS) variables are rejected by the nitrogen work hardening result to a large extent.

WAAM technology with PAW has high deposition rates and can producing components of various sizes and yields with high mechanical performance. Similarly, two walls of Ti6Al4V were fabricated in a shielding argon atmosphere using WAAM-PAW to examine the deposition process, the growth in height per layer, the temperature deposition process, and the cooling times, which gave good results [69]. Three-dimensional thermoelastic–plastic transients and the thermomechanical multi-layer wall structure modeling approach are studied in [30]. The result of the study shows that temperature simulations and distortion expectations are proved by equating with the experimental results of laser scanners and thermocouples, while the RS is verified using neutron diffraction of strain scanner ENGIN-X. The response of the mechanical to the thermal history is examined by performing a 3D quasi-static incremental analysis.

The yield strength (σ_y), elastic modulus (E), and coefficient of thermal expansion (α) are temperature-dependent, while other mechanical property values such as Poisson's ratio are independent of temperature [89]. The physical and mechanical behavior of temperature-dependent properties such as the thermal conductivity, specific heat, and yield stress of SAE-AISI 1524 steel were studied in [90]. For materials such as SS 316 L, the behavior is supposed to be elastoplastic with a mix of kinematic and isotropic hardening (Chaboche-

like model) [31]. Under the theory of small deformation, the total incremental strain can be disintegrated in elastic and inelastic forms. Equation (7) shows the formula for total deformation.

$$\Delta\varepsilon^{tot} = \Delta\varepsilon^{el} + \Delta\varepsilon^{th} + \Delta\varepsilon^{p} + \Delta\varepsilon^{vp} \tag{7}$$

where $\Delta\varepsilon^{el}$, $\Delta\varepsilon^{th}$, $\Delta\varepsilon^{p}$, and $\Delta\varepsilon^{vp}$ are, respectively, the elastic, thermal, plastic, and viscoplastic total incremental strains. The thermal strain is expressed in the absence of metallurgical transformations by Equation (8):

$$\varepsilon^{th} = \alpha(T)\left(T - T_{ref}\right) \tag{8}$$

where α is the thermal expansion coefficient and T_{ref} is a reference temperature. In all three directions, the strains measured were combined to analyze the stress, supposing the directions measured are given by Hooke's law with principal strain directions [30], as Equation (9).

$$\sigma_x = \frac{E}{(1+v)}\varepsilon_x + \frac{Ev}{(1+v)(1-2v)}\left(\varepsilon_x + \varepsilon_y + \varepsilon_z\right) \tag{9}$$

where ε_x, ε_y, and ε_z are strains in the principal directions, E is the modulus of elasticity, and v is Poisson's ratio of the material.

4. Analysis of Residual Stress Effects in WAAM Components

The RS in WAAM products exists due to non-uniform heating or cooling results and cannot be ignored [47]. However, there are techniques to print products using WAAM with the minimum amount of RS and distortion [91]. RS are inherent in parts manufactured using the WAAM method, resulting in unpredictable structural integrity, and a variety of mechanical responses are seen [36]. As reported in [92], a continuous tool-path in the process is one of the factors. RS analysis can be examined using FE modeling in the WAAM process, which is very important because of the influence of thermal loads on the mechanical properties and life cycle of the built parts that mostly rely on this RS [31,47,93]. Tensile RS in the WAAM process is induced along the weld bead. This is due to the input parameters [94], molten metal contraction, and the welding parameters [47]. On the another hand, material shrinkage during solidification causes compressive RS in the base plate [30,33].

Microstructures, mechanical properties, RS, and distortion of metals and their alloys in products made using the WAAM process are affected by the process parameters. Many investigations show that these parameters are the major factors used to improve the quality of manufactured components [32,95]. Furthermore, the defects are strictly associated with the target characteristics by the process parameters [13,96].

The causes of WAAM defects can be various, and for these reasons, the vulnerable material responses are different [6,47,96–99]. The reasons include unstable weld-pool-like dynamics due to poor parameter setup, poor software design strategy, thermal-deformation-related heat accumulation, environmental conditions, machine malfunctions, and others. Figure 4 illustrates some selected materials affected by specific defects. For instance, there is severe porosity for aluminum alloys, oxidation for titanium alloys, and poor roughness of the surface in steel, along with severe distortion and bimetal cracks [13].

Different process parameters and preheating strategies are sensitive to process assessment to check their helpfulness in the mitigation of RS and distortions [96]. The effects of the processing conditions such as the interlayer temperature, deposit height, and substrate thickness on the distribution and magnitude of RS were studied. The study results show that the thickness of the substrate was the main influence on the RS distribution along the height of the deposit. The major part of the substrate revealed recompensing compressive RS while the deposited layer shows tensile stress [100–102].
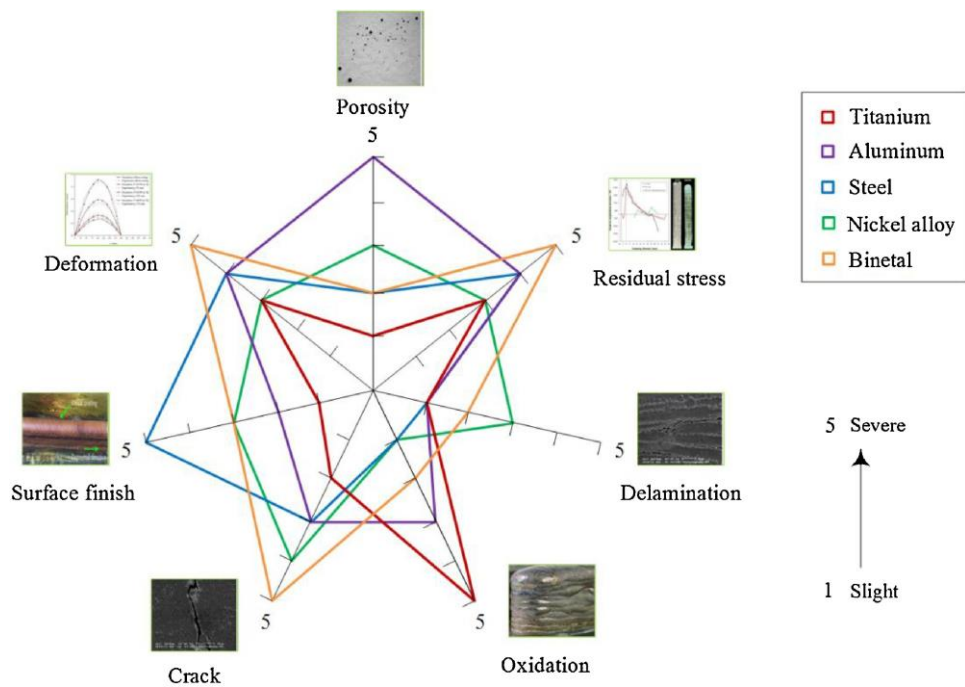
Figure 4. The relationship between defects and materials in WAAM processes (Reprinted with permission from ref. [13]. Copyright 2018, Elsevier, License Number-5479380307471).

4.1. Method of Measuring Residual Stress during and after Processing

Measuring RS physically is difficult and hence it is mostly estimated theoretically. Neutron diffraction and radiographic testing (X-ray) are the most common RS measurement tools using Bragg's law, and they reveal qualitative experimental results [73,103]. The procedure for RS measurement using the contour method is discussed in [104]. Figure 5 shows the three categories of RS measurement techniques: (1) destructive; (2) non-destructive; and (3) semi-destructive techniques [16,44,47,104–110].
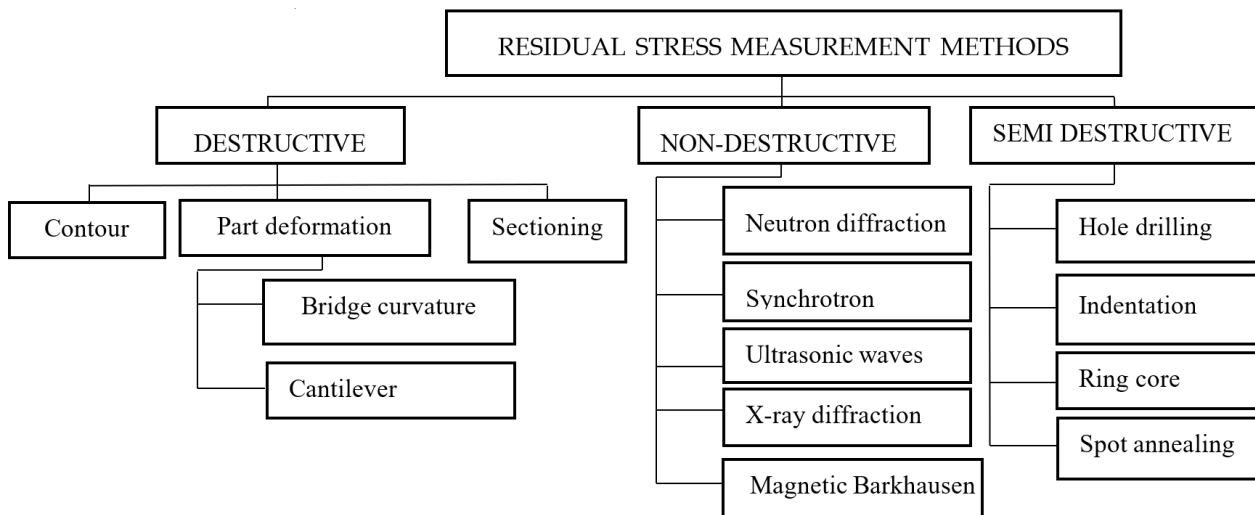
Figure 5. Categories of residual stress measurement methods (Reprinted with permission from ref. [104]. Copyright 2011. Elsevier, License Number-5481390488471).

The mechanisms of strengthening printed components using various post-processing methods are discussed in [48,97], while the study of the heat input effect on the evolution and control of RS in long-scale WAAM-fabricated components is reported in [79]. Based on

the analysis of RS distribution with Simufact 2016–FEA software, the clamping method with only the transverse direction can attain the least RS distribution [111]. The investigation reported by Nadeem and Ahmed [82] showed that high tensile stresses can be the cause of performance loss in fatigue, corrosion, and fracture. The experimental and FEA study results also indicated a good agreement for the anticipated RS and distortion, which showed a loss of measurements of performance in the WAAM products. According to Chi et al. [112], the RS results measured with the X-ray diffraction technique are used to examine the effects of path planning in the WAAM process.

4.2. Method of Minimizing Residual Stress and Distortion

Various RS- and distortion-mitigation methods are compiled in the WAAM process to deliver a framework direction for the future. Likewise, simulations validated with experimental results are examined depending on the thermal fields of RS and distortion to provide a critique of real-life tests [44,113]. Defects in WAAM can be reduced effectively by the form of reasonable clamping [111]. For instance, the laser cladding process (CLAD) was used to improve the distortions in the WAAM process, according to study results conducted on parts made of Ti–6Al–4V [106]. The peening effect, especially laser shock peening (LSP), is an innovative method to strain refinement and improve RS typically on the layer surface, as shown in Figure 6 [114]. While the enlarged images in Figure 6b–d, before LSP indicate existence of evenly distributed dimples and few micro-voids, the images after application of LSP (Figure 6f–h) show tearing ridges, cleavage steps and cleavage planes that are typical SEM fracture morphologies after such process [114]. Interpass cold rolling [115], weld pool oscillation, interpass cooling [5,76,116], and heat treatment [80,117,118] are also used to minimize RS in the WAAM components. Another method is reducing the layer thickness and deposition rate during WAAM, which significantly minimizes RS [50]. A thermomechanical model depending on 3D heat sources was developed by the Simufact 2016 welding software. The numerical model forecasted precisely the profile of the molten pool, the thermal cycles, and the distortion geometry of the butt weld, and an experimental test was carried out to determine the distortion, dimensions, and shape of the weld [77,119].

Rolling is an effective technique during printing processing that improves the mechanical properties by refining the grain size in WAAM-printed parts [36], as illustrated in Figure 7a [120]. Similarly, different RS- and distortion-mitigation methods performed in WAAM have been compiled to provide an outline for future research directions [44]. Mitigating RS and distortion is possible using active interpass cooling in the WAAM process [68,75,86]. In welding, ultrasonic impact treatment (UIT) is an effective method widely used for RS reduction and surface refinement, and similarly, investigations prove that UIT can be used in WAAM [121]. Several methods have been proposed by investigators to decrease RS during WAAM, including:

(1) high-pressure rolling with clamping [122], as illustrated in Figure 7b;
(2) air-jet impinging, as shown in Figure 7 [123];
(3) dwell time after layer deposition [124];
(4) machining between intermittent layers [108]; and
(5) laser shock peening [114].

Figure 8 illustrates an air-jet impinging system in a coolant hose that is connected to the welding torch and thus operates synchronously with it to cool the molten bead during the WAAM process. The air jet is conveyed by the hose nozzle to overthrow on the surface, as shown by the green highlighted area in Figure 8a under the welding torch, and the main geometric parameters are shown in Figure 8b. Heat transfer is modelled with Newton's law based on the fluid reference temperature and local surface temperature [124]. There are also other methods of cooling mechanisms that are used to minimize defects [63,125].
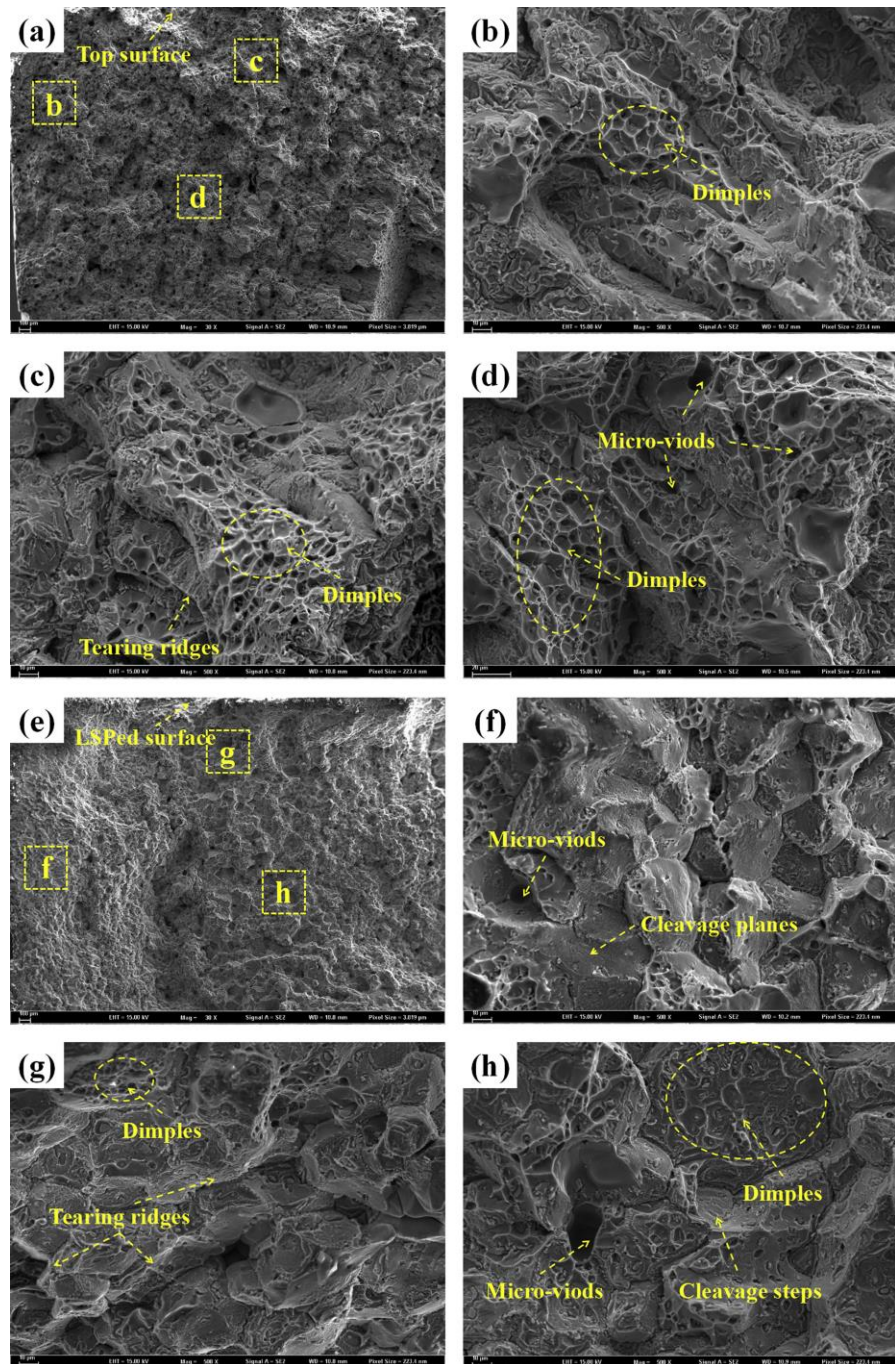
Figure 6. SEM fracture morphologies of specimens before and after LSP. (**a–d**) before LSP, and (**e–h**) after LSP. (Reprinted with permission from ref. [114]. Copyright 2018. Elsevier, License Number-5479380909594).

Recently, the hybrid methods that WAAM uses to manufacture the near net shape for the single-step with hot forging process were developed to overcome the defects and anisotropic properties of the products [126]. On the other hand, performing heat treatment and peening processes in WAAM showed that refinement occurred up to the first layer band in the microstructure. The smallest grains were observed just above the boundary at which higher temperatures and significant grain growth occurred [47,70,80,118].
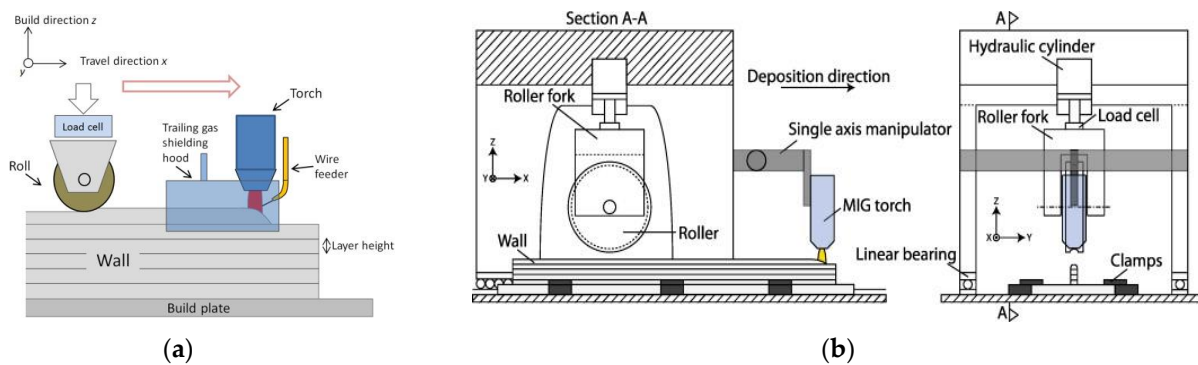
**Figure 7.** (**a**) Illustration of the combination of a rolling step sequentially with layer deposition and minimizing RS in the WAAM process (Reprinted with permission from ref. [121]. Copyright 2018. Elsevier, in accordance with CC BY license, Open access); and (**b**) Schematic illustration of rolling on printing and with clamps equipment (Reprinted with permission from ref. [122]. Copyright 2013. Elsevier, License Number-5493060104979).
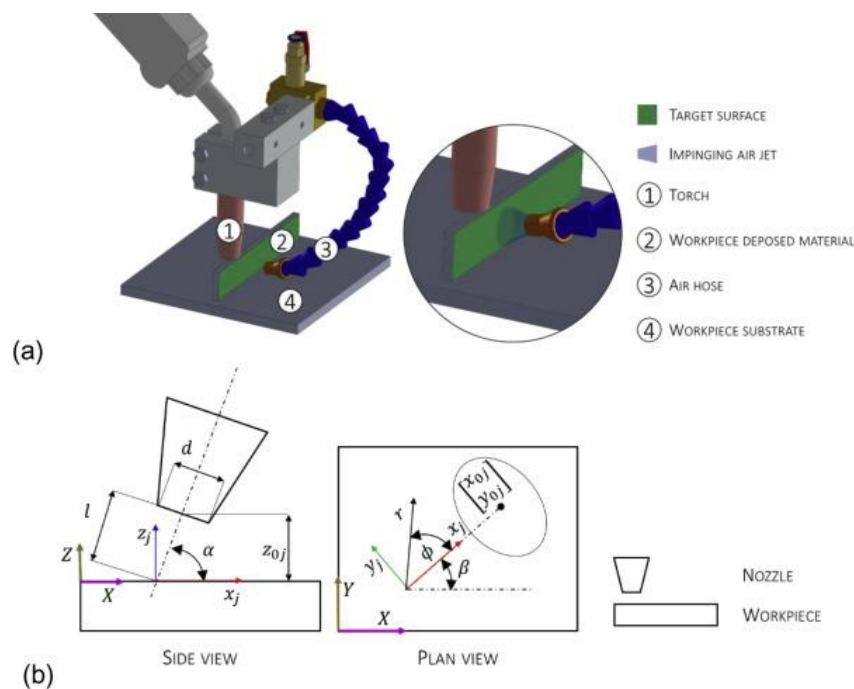
Figure 8. (**a**) The archetype of the proposed cooling system and (**b**) the geometric parameters of the jet-impingement model (Reprinted with permission from ref. [124]. Copyright 2018. Elsevier, License Number-5493050332263).

As illustrated in Figure 9 [48], several researchers used different methods of post-processing after completing the WAAM production to eliminate defects. These actions started by observing that defects are mainly minimized using several methods (Figure 9).

Among the methods used, some are used during and after the printing process to enhance the product quality. The main methods and parameters reported in diverse studies to enhance the required qualities and to minimize residual stress and distortion with their effects on printed parts are listed in Table 2.
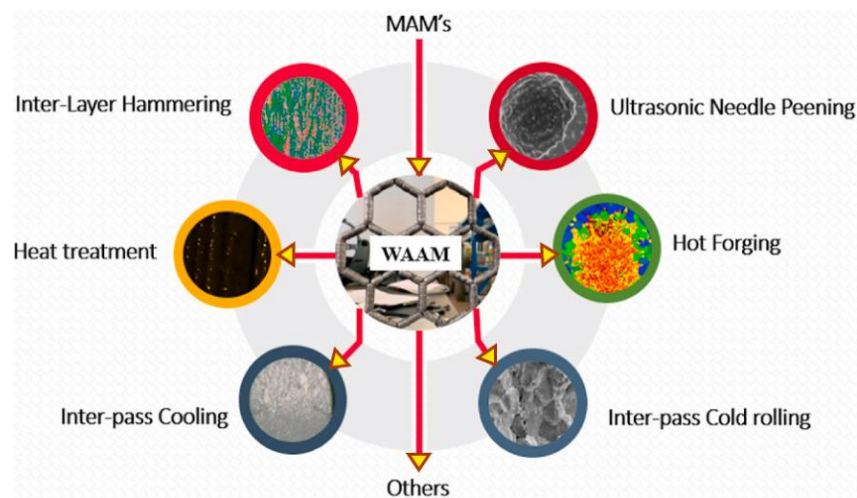
Figure 9. Collection of post-processing methods after WAAM (Reprinted with permission from ref. [48]. Copyright 2022. Elsevier, License Number-5493060104979).

Table 2. Methods and parameters for minimizing residual stress and distortion.

S/N	Methods	Parameters	Effect on Printed Parts	References
1	Clamping form (on edge and corner in the transverse and longitudinal direction)	Edges and corner clamping form force; longitudinal and transverse clamping form force	Reduce defects (RS and distortion)	[111,122]
2	Laser shock peening	Shallow thickness and size of microscopic voids	Ductile fracture existed in the specimen after LSP	[114,127]
3	Post-deposition heat treatments	Process parameters (travel speed, arc length, wire feed, current, and voltage) with single- and multi-weld beads.	Reduces anisotropy, increases elongation, mixed sub grain is visible	[124,128]
4	Post-process heat treatment	Temperature, material design, and other parameters	Grain refinement and improvement of material strength minimize residual stress, control hardness	[13,117]
5	Interpass Rolling	Temperature and the volume of the weld pool	Minimizes microstructural anisotropy via plastic deformation of the deposit; grain refinement; uniform layer height; increase in wall width; enhances the mechanical properties	[5,76,117,118]
6	Thermal monitoring	Distance of welding torch and parent material, temperature of the molten pool, weld pool area, and wavelength	Uniform microstructure, improved material properties, and reduced defects of parts	[24,39,129]
7	Active interpass cooling	Travel speed, cooling gas flow rate, and cooling time	Improved microhardness and mechanical strength, more fine-grained, more grain boundary high-density dislocations, and attain isotropic property	[71,130–132]
8	Vertical and pinch rolling processes	Rolling depth, curvature depth of the roller, roller shape, transverse displacement, rolling direction, and roller thickness	Refines the grains, minimizes voids, and enhances the mechanical properties	[36,54,72]
9	Interpass cold rolling	Deposited layer thickness, radius of roller, loads	Brings more homogeneous, large columnar grains; improves mechanical properties	[13,115]

Stress evolution analyzed theoretically for ribs along central lines was conducted without consideration of the distribution of stress hypothesis in the WAAM process [133]. The reported results showed that warpage and stress remain unmanageable problems.

According to this review, many investigations have been conducted on different techniques with various feedstock materials to determine RS and distortion in WAAM products. Similarly, experimental and numerical analyses for different feedstocks are presented with different results and explanations. Table 3 shows summaries of the general methods, feedstock materials, and their discussion of results used in WAAM processes.

Table 3. WAAM technologies' feedstock materials, methods, results, and discussions.

Feedstock Materials	Methods	Results and Explanation	Reference
Carbon steel	Numerical approach: ABAQUS software 2019	An increasing number of deposited layers increases the peak temperature. Preheating a substrate increases the peak temperature of the first layer and decreases its average cooling speed. The thermal behavior of deposited layers is mainly affected by the travel speed	[12]
AZ31-magnesium and G4Si1 (1.5130) for stainless steel materials.	FE software MSC Marc 2017 and experimental tests	Examined distortions, temperature fields, and mechanical properties. A uniform wall geometry can be formed using a continuous welding path with same temperature distribution	[53,134]
316 L stainless steel and Iron Aluminide (Fe_3Al)	Neutron diffraction and numerical analysis	Temperature and RS fields were computed at each time stage and more reliable RS results were obtained from the acquired neutron diffraction	[31,103,135]
Stainless steels 308LSi and 304	Thermomechanical coupling analysis model	RS in both structures and their relationship with the deposition height and shape were simulated; measured RS validated with simulation	[136]
A36 steel	DFLUX in ABAQUS analysis and experimental test	Both thermal and mechanical models were validated with the experimental data	[137]
Stainless steel alloy 304L	FEA software ABAQUS 2017	Influences of roller design, rolling load, and friction coefficient on plastic strain and RS distributions were analyzed and elucidated	[138]
Ti-6Al-4V	Experimental test (Neutron diffraction) and FEA	Contour method of RS measurements and micro-hardness measurements were in good agreement away from the baseplate. The results indicate that a measurement-based convection model is requisite to produce accurate simulation results. Built the single-bead walls with different process situations; RS was significantly minimized after substrate removing	[2,30,106, 139–141]
ER70S-6 commonly used welding wire	X-ray and neutron diffraction	The warpage and hardness have a direct relation with measured RS	[50]
Aluminum, silicon, and copper	Laser opto-ultrasonic dual-detection approach	Detected compositions of elemental, defects of structural, and RS in Al-alloy components during WAAM processes. LOUD detection holds the promise of becoming an effective testing method for WAAM processes to ensure quality control and process feedback	[142]
Aluminum and its alloys	Taguchi method and ANNOVA analysis: three process parameters: wire feed rate, gas flow rate, and welding speed	The correlations between the process variables and response variables were developed using the multiple regression method. Shows fine-grained microstructure and how it improves the properties of the modeled wall.	[143,144]

Table 3. *Cont.*

Feedstock Materials	Methods	Results and Explanation	Reference
AA6061, Aluminum	Neutron diffraction	RS measurements show tensile stresses (up to 130 MPa) in the built parts and compressive stresses (up to -80 MPa) in the substrate. Less copper in solid solution with aluminum, showing greater precipitation and so, potentially paying to improve the strength of the material.	[145,146]
Stainless steel	Numerical modeling software such as MSC Marc 2019/Mentat	The outcome of this research is to develop an effective procedure to analyze the distortion and RS of WAAM of stainless steel.	[53,93]
Grade 91 steel (P91)	Post-WAAM heat treatment process	The microstructure is optimized with a very fine martensite lath and rational prior austenite grain size (PAGS).	[147]
304 Stainless steel	COMSOL–5.4 Multiphysics software	Simulated the build-up of the wall. To validate this model, the dimensions of the melt pool and the shape of the deposit calculated for the first layer were compared to experimental data given by macrographs and high-speed videos.	[148]
Aluminum alloys	Experiments measure temperature results (thermal cycles, etc.)	Variation in the beam height can affect the measurement and longitudinal RS distribution in both the beam and the substrate, while that can only influence the transverse RS in the substrate but not in the beam nearly	[32,66]
Ti17 Titanium alloy	Post-treatment technique combining laser shock peening and heat treatment	Enhance the mechanical performance of WAAM parts by changing their microstructure and RS distribution	[127]
Nickel-based super alloys	X-ray, optical, and scanning electron microscopy	Studied the microstructure, RS, and mechanical properties	[149]
Ti-6Al-4V and Inconel 718	Hole-drilling method, theoretical and experimentally	RS and distortion were minimized by printing with short track lengths among the three patterns investigated for both alloys. The strain parameter exactly predicted the effects of WAAM parameters on distortion when the detailed thermomechanical calculations cannot be carried out	[19,143]
Aluminum	Finite element model and experiments	Predicted the melt pool volume as an indicator of the porosity rate	[150]
Ti-6Al-4V	Thermocouple measurements and numerical simulation	Measured and predicted temperatures, RS, and distortion profiles indicated that the model is quite reliable for grain morphology, predicting the cooling rates and the microstructure	[33]

5. Discussion

This section mostly discusses the limitations of thermomechanical modeling and methods of minimizing RS carried out in the past literature that is used in this review article. As the use of thermomechanical modeling for WAAM products is a major contributor to the increase in the quality of the part, it is important to control RS and distortion. Although WAAM technology is used in various application areas, it is very applicable in the aerospace, automotive, and defense industries. These applications require very intensive consideration of the components due to the RS and distortion as a result of thermal stress. In this review, the most widely seen problems during thermomechanical modeling are in the case of multi-joint printed parts. At the multi-joint places, there are additional heat effects that alter the first deposition behavior of the parts. For instance, if one component with the

shape of the cross is printed using the WAAM process, the joint place is repeatedly affected by thermal loads. Nevertheless, the investigators have not considered thermal modeling for such occurrences that produce non-uniform thermal stress and dissimilar properties through printed parts, which leads to unpredicted failure. Out of all the articles used in this review, none of them considers thermomechanical modeling for irregular shapes and multi-jointed components' effects on RS and distortion in the WAAM process.

The control and prediction of the evolution of microstructural behaviors, which are responsible for the deviation of mechanical properties for WAAM-printed components, are big challenges since thermal processes are inherently non-equilibrium. In such cases, there are no clear control mechanisms to obtain an optimum RS and distortion in the WAAM products. Similarly, in the long-path and short-path depositing processes, the RS and distortion induced in the part varies due to variation in the time it takes to add consecutive deposition layers. The deposits of short paths faced redundant heat effects, while long paths release the heat from molten beads since they have more time for cooling. Additionally, parameters such as the width and thickness of deposition beads are also important for heat release, with the length component, which varies the volume of deposited beads, and the time it has taken to deposit consecutive layers. Therefore, consideration of parameters such as the length, width, and depth (thickness) of deposition leads to good results for thermomechanical modeling to determine RS and distortion in the printed parts [151].

In the case of the substrate (base plate), the literature explains that the thickness of the substrate has effects on RS and distortion. This is due to heat conduction loss during printing, which leads to variation in the heat movements in the molten bead deposited. Likewise, pre-heating the substrate makes it smoother and decreases the cooling rate of the molten pool. Nevertheless, the dependence of temperature magnitude on the pre-heating substrate is not specified [74]. The optimum temperature and specific substrate thickness for each printed metal or alloy material have not yet been stated with regard to the printed thickness.

In other ways, the thermomechanical modeling conducted in the reviewed articles has not considered the wire diameter being used in the depositing process. The wire used for WAAM processes is available in different diameters, which can contribute to variation in the distortion during printing. The trial was performed using different diameters—0.8 mm and 1.2 mm—to test humping effect dependence. From the results, less humping was seen in 0.8 mm wire than in 1.2 mm [152]. However, the effects of wire diameter variation on RS are not mentioned in all reviewed articles. For a known wire diameter, printing layer thickness, and standard feeding rate, it is possible to predict the RS and distortion using the thermomechanical modeling of WAAM.

RS and distortion induced in WAAM products are closely related to the specific process parameters and material characteristics. Thus, the chemical composition of the wire and the physical mechanisms should be considered as further research in the thermomechanical modeling of the WAAM process to optimize the defects of the products. Understanding the thermomechanical effects should be ancillary to strategies for development of WAAM process since it is the major important factor to overcome the generation of defects. Nevertheless, no preferential consistency was clearly stated and developed to obtain optimum RS and distortion. Furthermore, in order to conduct research on the thermomechanical effect of WAAM processes, an understanding of the thermal cycles in the process and materials' thermal characteristics is very crucial for printing defect-free products. Since different materials perform differently in similar conditions, there would be various specifications used for different materials.

RS and distortions are mitigated using various methods. Among all methods mentioned in Section 4.2, clamping and interpass rolling are limited only in the case of regularly shaped parts. For parts with an irregular shape, these mechanisms of minimizing RS and distortion are not relevant due to the constraints of disallowing of the geometry of the component. Further investigations in thermomechanical modeling would be recommended to

consider the hindered concepts, such as multi-joints, length of deposition path, pre-heated substrate, and wire diameter.

6. Conclusions

This review article presented the details of thermomechanical modeling and analysis of RS with a focus on how the thermal input effects are interrelated to the mechanical properties and RS associated with the WAAM process, as well as the characterization of the products. According to the literature reviewed, the mechanical performance of WAAM components is determined by defects that exist in the products, which are mostly affected by the thermal cycle performed during the manufacturing process.

Thermal loads that affect WAAM products are divided into two categories: (1) thermal load effects during the manufacturing process and (2) thermal load effects during post-processing (heat treatment) on the products. Even though both contribute to the RS in the products, a greater effect on products is observed from the first one. While the first thermal load type is intended to give the heat input needed for wire melting at the time of the fabrication process, the second load is to strengthen the product after it is printed. In these two cases, the thermal characterization of materials is very useful because it is related to the composition of the material and its microstructure, which govern the properties of the material and fabrication quality. All metals have no identical melting point and can have various molten densities, which causes changes in the mechanical and thermal properties of the products. The deposition plan and rolling of interlayers are the best-adopted RS- and distortion-mitigation methods in WAAM products up to the present time. As confirmed from the literature review, the mechanical and thermal characterization of the printed materials are affected by the heat input for the WAAM process. Accordingly, our future research on this topic will focus on the observed research gaps such as the influence of the wire diameter, substrate temperature, and length of the deposition layers on the reduction of defects.

Author Contributions: Conceptualization, F.D.G. and H.G.L.; methodology, F.D.G.; software, F.D.G.; validation, H.G.L.; formal analysis, F.D.G.; investigation, F.D.G.; resources, H.G.L.; data curation, F.D.G.; writing—original draft preparation, F.D.G.; writing—review and editing, H.G.L.; visualization, F.D.G. and H.G.L.; supervision, H.G.L.; project administration, H.G.L.; funding acquisition, H.G.L. All authors have read and agreed to the published version of the manuscript.

Institutional Review Board Statement: Not applicable.

Informed Consent Statement: Not applicable.

Data Availability Statement: Not applicable.

Conflicts of Interest: The authors declare no conflict of interest.

References

1. Ding, J.; Williams, S.W. Thermo-mechanical Analysis of Wire and Arc Additive Manufacturing Process. Ph.D. Thesis, Cranfield University, Bedford, UK, 2012; pp. 40–187.
2. Williams, S.W.; Martina, F.; Addison, A.C.; Ding, J.; Pardal, G.; Colegrove, P. Wire + Arc additive manufacturing. *Mater. Sci. Technol.* **2016**, *32*, 641–647. [CrossRef]
3. Ho, A.; Zhao, H.; Fellowes, J.W.; Martina, F.; Davis, A.E.; Prangnell, P.B. On the origin of microstructural banding in Ti-6Al4V wire-arc based high deposition rate additive manufacturing. *Acta Mater.* **2019**, *166*, 306–323. [CrossRef]
4. Müller, J.; Grabowski, M.; Müller, C.; Hensel, J.; Unglaub, J.; Thiele, K.; Dilger, K. Design and parameter identification of wire and arc additively manufactured (WAAM) steel bars for use in construction. *Metals* **2019**, *9*, 725. [CrossRef]
5. Chaturvedi, M.; Scutelnicu, E.; Rusu, C.C.; Mistodie, L.R.; Mihailescu, D.; Arungalai Vendan, S. Wire arc additive manufacturing: Review on recent findings and challenges in industrial applications and materials characterization. *Metals* **2021**, *11*, 939. [CrossRef]
6. Barath Kumar, M.D.; Manikandan, M. Assessment of Process, Parameters, Residual Stress Mitigation, Post Treatments and Finite Element Analysis Simulations of Wire Arc Additive Manufacturing Technique. *Met. Mater. Int.* **2022**, *28*, 54–111. [CrossRef]

7. Mansoor, O.; Wahdatullah, N.; Harshavardhana, N. Wire Arc Additive Manufacturing (WAAM) of Inconel 625 Alloy and its Microstructure and Mechanical Properties. *Int. Res. J. Eng. Technol.* **2021**, *8*, 1517–1528.

8. Rusteiko, A.C.; Angelo, J.D.; del Conte, E.G.D. Residual stress in metal arc additive manufacturing of mill knives cutting edges. *Int. J. Adv. Manuf. Technol.* **2019**, *104*, 4457–4464. [CrossRef]

9. Wu, Q.; Mukherjee, T.; De, A.; DebRoy, T. Residual stresses in wire-arc additive manufacturing—Hierarchy of influential variables. *Addit. Manuf.* **2020**, *35*, 101355. [CrossRef]

10. Ding, D.; Zhang, S.; Lu, Q.; Pan, Z.; Li, H.; Wang, K. The well-distributed volumetric heat source model for numerical simulation of wire arc additive manufacturing process. *Mater. Today Commun.* **2021**, *27*, 102430. [CrossRef]

11. Oyama, K.; Diplas, S.; M'hamdi, M.; Gunnæs, A.E.; Azar, A.S. Heat source management in wire-arc additive manufacturing process for Al-Mg and Al-Si alloys. *Addit. Manuf.* **2019**, *26*, 180–192. [CrossRef]

12. Saadatmand, M.; Talemi, R. Study on the thermal cycle of wire arc additive manufactured (WAAM) carbon steel wall using numerical simulation. *Frat. Ed. Integrita Strutt.* **2020**, *14*, 98–104. [CrossRef]

13. Wu, B.; Pan, Z.; Ding, D.; Cuiuri, D.; Li, H.; Xu, J.; Norrish, J. A review of the wire arc additive manufacturing of metals: Properties, defects and quality improvement. *J. Manuf. Process.* **2018**, *35*, 127–139. [CrossRef]

14. Li, R.; Xiong, J.; Lei, Y. Investigation on thermal stress evolution induced by wire and arc additive manufacturing for circular thin-walled parts. *J. Manuf. Process.* **2019**, *40*, 59–67. [CrossRef]

15. Wu, B.; Pan, Z.; Ding, D.; Cuiuri, D.; Li, H. Effects of heat accumulation on microstructure and mechanical properties of Ti6Al4V alloy deposited by wire arc additive manufacturing. *Addit. Manuf.* **2018**, *23*, 151–160. [CrossRef]

16. Shen, C.; Ma, Y.; Reid, M.; Pan, Z.; Hua, X.; Cuiuri, D.; Paradowska, A.; Wand, L.; Li, H. Neutron diffraction residual stress determinations in titanium aluminide component fabricated using the twin wire-arc additive manufacturing. *J. Manuf. Process.* **2022**, *74*, 141–150. [CrossRef]

17. Ding, D.; Pan, Z.; Cuiuri, D.; Li, H. Wire-feed additive manufacturing of metal components: Technologies, developments and future interests. *Int. J. Adv. Manuf. Technol.* **2015**, *81*, 465–481. [CrossRef]

18. Köhler, M.; Hensel, J.; Dilger, K. Effects of thermal cycling on wire and arc additive manufacturing of al-5356 components. *Metals* **2020**, *10*, 952. [CrossRef]

19. Youheng, F.; Guilan, W.; Haiou, Z.; Liye, L. Optimization of surface appearance for wire and arc additive manufacturing of Bainite steel. *Int. J. Adv. Manuf. Technol.* **2017**, *91*, 301–313. [CrossRef]

20. Ou, W.; Mukherjee, T.; Knapp, G.L.; Wei, Y.; DebRoy, T. Fusion zone geometries, cooling rates and solidification parameters during wire arc additive manufacturing. *Int. J. Heat Mass. Transf.* **2018**, *127*, 1084–1094. [CrossRef]

21. Li, J.L.Z.; Alkahari, M.R.; Rosli, N.A.B.; Hasan, R.; Sudin, M.N.; Ramli, F.R. Review of wire arc additive manufacturing for 3d metal printing. *Int. J. Autom. Technol.* **2019**, *13*, 346–353. [CrossRef]

22. Evjemo, L.D.; Langelandsvik, G.; Moe, S.; Danielsen, M.H.; Gravdahl, J.T. Wire-arc additive manufacturing of structures with overhang: Experimental results depositing material onto fixed substrate. *CIRP J. Manuf. Sci. Technol.* **2022**, *38*, 186–203. [CrossRef]

23. Wu, B.; Pan, Z.; Chen, G.; Ding, D.; Yuan, L.; Cuiuri, D.; Li, H. Mitigation of thermal distortion in wire arc additively manufactured Ti6Al4V part using active interpass cooling. *Sci. Technol. Weld. Join.* **2019**, *24*, 484–494. [CrossRef]

24. Baier, D.; Wolf, F.; Weckenmann, M.; Zaeh, M.F. Thermal process monitoring and control for a near-net-shape Wire and Arc Additive Manufacturing. *Prod. Eng.* **2022**, *16*, 811–822. [CrossRef]

25. Srivastava, S.; Garg, R.K.; Sachdeva, A.; Sharma, V.S. Distribution of Residual Stress in Wire-Arc Additively Manufactured Small-Scale Component: Single- Versus Multi-Level Heat Input. *J. Manuf. Sci. Eng.* **2022**, *145*, 021008. [CrossRef]

26. Veiga, F.; Suárez, A.; Artaza, T.; Aldalur, E. Efect of the Heat Input on Wire-Arc Additive Manufacturing of Invar 36 Alloy: Microstructure and Mechanical Properties. *Weld. World* **2022**, *66*, 1081–1091. [CrossRef]

27. Pixner, F.; Buzolin, R.; Schönfelder, S.; Theuermann, D.; Warchomicka, F.; Enzinger, N. Contactless temperature measurement in wire-based electron beam additive manufacturing Ti-6-Al-4V. *Weld. World* **2021**, *65*, 1307–1322. [CrossRef]

28. Rodrigues, T.A.; Duarte, V.; Avila, J.A.; Santos, T.G.; Miranda, R.M.; Oliveira, J.P. Wire and arc additive manufacturing of HSLA steel: Effect of thermal cycles on microstructure and mechanical properties. *Addit. Manuf.* **2019**, *27*, 440–450. [CrossRef]

29. Nagasai, B.P.; Malarvizhi, S.; Balasubramanian, V. Effect of welding processes on mechanical and metallurgical characteristics of carbon steel cylindrical components made by wire arc additive manufacturing (WAAM) technique. *CIRP J. Manuf. Sci. Technol.* **2022**, *36*, 100–116. [CrossRef]

30. Ding, J.; Colegrove, P.; Mehnen, J.; Ganguly, S.; Almeida, P.M.S.; Wang, F.; Williams, S. Thermo-mechanical analysis of Wire and Arc Additive Layer Manufacturing process on large multi-layer parts. *Comput. Mater. Sci.* **2011**, *50*, 3315–3322. [CrossRef]

31. Cambon, C.; Rouquette, S.; Bendaoud, I.; Bordreuil, C.; Wimpory, R.; Soulié, F. Thermo-mechanical simulation of overlaid layers made with wire + arc additive manufacturing and GMAW-cold metal transfer. *Weld. World* **2020**, *64*, 1427–1435. [CrossRef]

32. Thapliyal, S. Challenges associated with the wire arc additive manufacturing (WAAM) of aluminum alloys. *Mater. Res. Express.* **2019**, *6*, 112006. [CrossRef]

33. Sikan, F.; Wanjara, P.; Gholipour, J.; Kumar, A.; Brochu, M. Thermo-mechanical modeling of wire-fed electron beam additive manufacturing. *Materials* **2021**, *14*, 911. [CrossRef] [PubMed]

34. Cui, J.; Yuan, L.; Commins, P.; He, F.; Wang, J.; Pan, Z. WAAM process for metal block structure parts based on mixed heat input. *Int. J. Adv. Manuf. Technol.* **2021**, *113*, 503–521. [CrossRef]

35. Chergui, A.; Villeneuve, F.; Béraud, N.; Vignat, F. Thermal simulation of wire arc additive manufacturing: A new material deposition and heat input modelling. *Int. J. Interact. Des. Manuf.* **2022**, *16*, 227–237. [CrossRef]

36. Tangestani, R.; Farrahi, G.H.; Shishegar, M.; Aghchehkandi, B.P.; Ganguly, S.; Mehmanparast, A. Effects of Vertical and Pinch Rolling on Residual Stress Distributions in Wire and Arc Additively Manufactured Components. *J. Mater. Eng. Perform.* **2020**, *29*, 2073–2084. [CrossRef]

37. Geng, H.; Li, J.; Xiong, J.; Lin, X.; Zhang, F. Optimization of wire feed for GTAW based additive manufacturing. *J. Mater. Process. Technol.* **2017**, *243*, 40–47. [CrossRef]

38. Goulas, A.; Southcott-Engstrøm, D.; Friel, R.J.; Harris, R.A. Investigation of additive manufacture of extra-terrestrial materials. In Proceedings of the 26th Annual International Solid Freeform Fabrication Symposium—An Additive Manufacturing Conference Reviewed Paper, Austin, TX, USA, 10–12 August 2015; pp. 2271–2281.

39. Carter, W.; Masuo, C.; Nycz, A.; Noakes, M.; Vaughan, D. Thermal process monitoring for wire-arc additive manufacturing using IR cameras. In Proceedings of the 30th Annual International Solid Freeform Fabrication Symposium—An Additive Manufacturing Conference Reviewed Paper, Austin, TX, USA, 8–10 August 2019; pp. 1812–1817.

40. Israr, R.; Buhl, J.; Bambach, M. A study on power-controlled wire-arc additive manufacturing using a data-driven surrogate model. *Int. J. Adv. Manuf. Technol.* **2021**, *117*, 2133–2147. [CrossRef]

41. Yang, Y.; Zhou, X.; Li, Q.; Ayas, C. A computationally efficient thermo-mechanical model for wire arc additive manufacturing. *Addit. Manuf.* **2021**, *46*, 102090. [CrossRef]

42. Bui, M.C.; Pham, T.Q.D.; Tran, H.S.; Van Tran, X. Efficient prediction of thermal history in wire and arc-directed energy deposition combining machine learning and numerical simulation. *Res. Sq.* **2022**, *23*, 0–23.

43. Treutler, K.; Wesling, V. The current state of research of wire arc additive manufacturing (Waam): A review. *Appl. Sci.* **2021**, *11*, 8619. [CrossRef]

44. Srivastava, S.; Garg, R.K.; Sharma, V.S.; Sachdeva, A. Measurement and Mitigation of Residual Stress in Wire-Arc Additive Manufacturing: A Review of Macro-Scale Continuum Modelling Approach. *Arch. Comput. Methods Eng.* **2021**, *28*, 3491–3515. [CrossRef]

45. Cao, H.; Huang, R.; Yi, H.; Liu, M.L.; Jia, L. Asymmetric molten pool morphology in wire-arc directed energy deposition: Evolution mechanism and suppression strategy. *Addit. Manuf.* **2022**, *59*, 03113. [CrossRef]

46. Zhou, Z.; Shen, H.; Lin, J.; Liu, B.; Sheng, X. Continuous tool-path planning for optimizing thermo-mechanical properties in wire-arc additive manufacturing: An evolutional method. *J. Manuf. Process.* **2022**, *83*, 354–373. [CrossRef]

47. Derekar, K.S. Aspects of Wire Arc Additive Manufacturing (WAAM) of Alumnium Alloy 5183. Ph.D. Thesis, Coventry University, Coventry, UK, 2020; pp. 1–227.

48. Kumar, N.; Bhavsar, H.; Mahesh, P.V.S.; Srivastava, A.K.; Bora, B.J.; Saxena, A.; Dixit, A.R. Wire Arc Additive Manufacturing—A revolutionary method in additive manufacturing. *Mater. Chem. Phys.* **2022**, *285*, 126144. [CrossRef]

49. Jafari, D.; Vaneker, T.H.J.; Gibson, I. Wire and arc additive manufacturing: Opportunities and challenges to control the quality and accuracy of manufactured parts. *Mater. Des.* **2021**, *202*, 109471. [CrossRef]

50. Singh, C.P.; Sarma, R.; Kapil, S. The qualitative analysis of warpage on residual stresses in wire arc additive manufacturing. *Mater. Today Proc.* **2022**, *62*, 6619–6627. [CrossRef]

51. Feng, G.; Wang, H.; Wang, Y.; Deng, D.; Zhang, J. Numerical Simulation of Residual Stress and Deformation in Wire Arc Additive Manufacturing. *Crystals* **2022**, *12*, 803. [CrossRef]

52. Gornyakov, V.; Sun, Y.; Ding, J.; Williams, S. Efficient determination and evaluation of steady-state thermal-mechanical variables generated by wire arc additive manufacturing and high pressure rolling. *Model. Simul. Mater. Sci. Eng.* **2022**, *30*, 014001. [CrossRef]

53. Ahmad, S.N.; Manurung, Y.H.P.; Mat, M.F.; Minggu, Z.; Jaffar, A.; Pruller, S.; Leitner, M. FEM simulation procedure for distortion and residual stress analysis of wire arc additive manufacturing. *IOP Conf. Ser. Mater. Sci. Eng.* **2020**, *834*, 012083. [CrossRef]

54. Belhadj, M.; Werda, S.; Belhadj, A.; Kromer, R.; Darnis, P. Thermal analysis of wire arc additive manufacturing process. In Proceedings of the 24th International Conference on Material Forming 2021, Liège, Belgium, 14–16 April 2021; pp. 2018–2022.

55. Montevecchi, F.; Venturini, G.; Scippa, A.; Campatelli, G. Finite Element Modelling of Wire-arc-additive-manufacturing Process. *Procedia CIRP* **2016**, *55*, 109–114. [CrossRef]

56. Wu, B.; Ding, D.; Pan, Z.; Cuiuri, D.; Li, H.; Han, J.; Fei, Z. Effects of heat accumulation on the arc characteristics and metal transfer behavior in Wire Arc Additive Manufacturing of Ti6Al4V. *J. Mater. Process. Technol.* **2017**, *250*, 304–312. [CrossRef]

57. Wu, B.; Pan, Z.; van Duin, S.; Li, H. *Thermal Behavior in Wire Arc Additive Manufacturing: Characteristics, Effects and Control*; Springer: Singapore, 2019.

58. Dharmendra, C.; Shakerin, S.; Ram, G.D.J.; Mohammadi, M. Wire-arc additive manufacturing of nickel aluminum bronze/stainless steel hybrid parts interfacial characterization, prospects, and problems. *Materialia* **2020**, *13*, 100834. [CrossRef]

59. Park, J.; Lee, S.H. Cmt-based wire arc additive manufacturing using 316l stainless steel (2): Solidification map of the multilayer deposit. *Metals* **2021**, *11*, 1725. [CrossRef]

60. Geng, H.; Li, J.; Xiong, J.; Lin, X. Optimisation of interpass temperature and heat input for wire and arc additive manufacturing 5A06 aluminium alloy. *Sci. Technol. Weld. Join.* **2017**, *22*, 472–483. [CrossRef]

61. Ou, W.; Knapp, G.L.; Mukherjee, T.; Wei, Y.; DebRoy, T. An improved heat transfer and fluid flow model of wire-arc additive manufacturing. *Int. J. Heat Mass. Transf.* **2021**, *167*, 120835. [CrossRef]

62. Rosli, N.A.; Alkahari, M.R.; bin Abdollah, M.F.; Maidin, S.; Ramli, F.R.; Herawan, S.G. Review on effect of heat input for wire arc additive manufacturing process. *J. Mater. Res. Technol.* **2021**, *11*, 2127–2145. [CrossRef]

63. Li, F.; Chen, S.; Shi, J.; Zhao, Y.; Tian, H. Thermoelectric cooling-aided bead geometry regulation in wire and arc-based additive manufacturing of thin-walled structures. *Appl. Sci.* **2018**, *8*, 207. [CrossRef]

64. Panchenko, O.; Kladov, I.; Kurushkin, D.; Zhabrev, L.; Ryl'kov, E.; Zamozdra, M. Effect of thermal history on microstructure evolution and mechanical properties in wire arc additive manufacturing of HSLA steel functionally graded components. *Mater. Sci. Eng. A* **2022**, *851*, 143569. [CrossRef]

65. Chen, S.; Xu, M.; Yuan, T.; Jiang, X.; Zhang, H.; Zheng, X. Thermal–microstructural analysis of the mechanism of liquation cracks in wire-arc additive manufacturing of Al–Zn–Mg–Cu alloy. *J. Mater. Res. Technol.* **2022**, *16*, 1260–1271. [CrossRef]

66. Sun, J.; Hensel, J.; Köhler, M.; Dilger, K. Residual stress in wire and arc additively manufactured aluminum components. *J. Manuf. Process.* **2021**, *65*, 97–111. [CrossRef]

67. Ríos, S.; Colegrove, P.A.; Martina, F.; Williams, S.W. Analytical process model for wire + arc additive manufacturing. *Addit. Manuf.* **2018**, *21*, 651–657. [CrossRef]

68. Derekar, K.; Lawrence, J.; Melton, G.; Addison, A.; Zhang, X.; Xu, L. Influence of Interpass Temperature on Wire Arc Additive Manufacturing (WAAM) of Aluminium Alloy Components. *MATEC Web. Conf.* **2019**, *269*, 05001. [CrossRef]

69. Scotti, F.M.; Teixeira, F.R.; da Silva, L.J.; de Araújo, D.B.; Reis, R.P.; Scotti, A. Thermal management in WAAM through the CMT Advanced process and an active cooling technique. *J. Manuf. Process.* **2020**, *57*, 23–35. [CrossRef]

70. Hönnige, J.; Colegrove, P.; Prangnell, P.; Ho, A.; Williams, S. The Effect of Thermal History on Microstructural Evolution, Cold-Work Refinement and {\alpha}/\b{eta} Growth in Ti-6Al-4V Wire + Arc AM. *arXiv* **2018**, preprint. arXiv:1811.02903.

71. Kozamernik, N.; Bračun, D.; Klobčar, D. WAAM system with interpass temperature control and forced cooling for near-net-shape printing of small metal components. *Int. J. Adv. Manuf. Technol.* **2020**, *110*, 1955–1968. [CrossRef]

72. Singh, S.; Jinoop, A.N.; Tarun Kumar, G.T.A.; Palani, I.A.; Paul, C.P.; Prashanth, K.G. Effect of interlayer delay on the microstructure and mechanical properties of wire arc additive manufactured wall structures. *Materials* **2021**, *14*, 4187. [CrossRef]

73. Lopez, A.; Bacelar, R.; Pires, I.; Santos, T.G.; Sousa, J.P.; Quintino, L. Non-destructive testing application of radiography and ultrasound for wire and arc additive manufacturing. *Addit. Manuf.* **2018**, *21*, 298–306. [CrossRef]

74. Köhler, M.; Sun, L.; Hensel, J.; Pallaspuro, S.; Kömi, J.; Dilger, K.; <monospace> </monospace>Zhang, Z. Comparative study of deposition patterns for DED-Arc additive manufacturing of Al-4046. *Mater. Des.* **2021**, *210*, 110122. [CrossRef]

75. Jorge, V.L.; Teixeira, F.R. Pyrometrical Interlayer Temperature Measurement in WAAM of Thin Wall: Strategies, Limitations and Functionality. *Metals* **2022**, *12*, 765. [CrossRef]

76. Richter, A.; Gehling, T.; Treutler, K.; Wesling, V.; Rembe, C. Real-time measurement of temperature and volume of the weld pool in wire-arc additive manufacturing. *Meas. Sensors* **2021**, *17*, 100060. [CrossRef]

77. Mohebbi, M.S.; Kühl, M.; Ploshikhin, V. A thermo-capillary-gravity model for geometrical analysis of single-bead wire and arc additive manufacturing (WAAM). *Int. J. Adv. Manuf. Technol.* **2020**, *109*, 877–891. [CrossRef]

78. Artaza, T.; Suárez, A.; Veiga, F.; Braceras, I.; Tabernero, I.; Larrañaga, O.; Lamikiz, A. Wire arc additive manufacturing Ti6Al4V aeronautical parts using plasma arc welding: Analysis of heat-treatment processes in different atmospheres. *J. Mater. Res. Technol.* **2020**, *9*, 15454–15466. [CrossRef]

79. Srivastava, S.; Garg, R.K.; Sachdeva, A.; Sharma, V.S. A multi-tier layer-wise thermal management study for long-scale wire-arc additive manufacturing. *J. Mater. Process. Technol.* **2022**, *306*, 117651. [CrossRef]

80. Seow, C.E.; Coules, H.E.; Wu, G.; Khan, R.H.U.; Xu, X.; Williams, S. Wire + Arc Additively Manufactured Inconel 718: Effect of post-deposition heat treatments on microstructure and tensile properties. *Mater. Des.* **2019**, *183*, 108157. [CrossRef]

81. Vishnukumar, M.; Muthupandi, V.; Jerome, S. Effect of post-heat treatment on the mechanical and corrosion behaviour of SS316L fabricated by wire arc additive manufacturing. *Mater. Lett.* **2022**, *307*, 131015. [CrossRef]

82. Nadeem, M.F.; Ahmed, B. Thermo-Mechanical Modelling and Experimental Verification of Distortion and Residual Stress for S355J2G3 Plate Welded by using Different Filler. *J. Sp. Technol.* **2019**, *9*, 71–82.

83. Chen, S.; He, T.; Wu, X.; Lei, G. Synergistic effect of carbides and residual strain on the mechanical behavior of Ni-17Mo-7Cr superalloy made by wire-arc additive manufacturing. *Mater. Lett.* **2021**, *287*, 129291. [CrossRef]

84. Hejripour, F.; Binesh, F.; Hebel, M.; Aidun, D.K. Thermal modeling and characterization of wire arc additive manufactured duplex stainless steel. *J. Mater. Process. Technol.* **2019**, *272*, 58–71. [CrossRef]

85. Bonifaz, E.A. Modelling of Thermal Transport in Wire + Arc Additive Manufacturing Process. *Lect. Notes Comput. Sci.* **2019**, *11539*, 647–659.

86. da Silva, L.J.; Souza, D.M.; de Araújo, D.B.; Reis, R.P.; Scotti, A. Concept and validation of an active cooling technique to mitigate heat accumulation in WAAM. *Int. J. Adv. Manuf. Technol.* **2020**, *107*, 2513–2523. [CrossRef]

87. Jimenez, X.; Dong, W.; Paul, S.; Klecka, M.A.; To, A.C. Residual Stress Modeling with Phase Transformation for Wire Arc Additive Manufacturing of B91 Steel. *Jom* **2020**, *72*, 4178–4186. [CrossRef]

88. Zhang, X.; Wang, K.; Zhou, Q.; Ding, J.; Ganguly, S.; Grasso, M.; Williams, S. Microstructure and mechanical properties of TOP-TIG-wire and arc additive manufactured super duplex stainless steel (ER2594). *Mater. Sci. Eng. A* **2019**, *762*, 138097. [CrossRef]

89. Norrish, J.; Polden, J.; Richardson, I. A review of wire arc additive manufacturing: Development, principles, process physics, implementation and current status. *J. Phys. D. Appl. Phys.* **2021**, *54*, 473001. [CrossRef]

90. Bonifaz, E.A.; Palomeque, J.S. A mechanical model in wire + Arc additive manufacturing process. *Prog. Addit. Manuf.* **2020**, *5*, 163–169. [CrossRef]

91. Huang, H.; Ma, N.; Chen, J.; Feng, Z.; Murakawa, H. Toward large-scale simulation of residual stress and distortion in wire and arc additive manufacturing. *Addit. Manuf.* **2020**, *34*, 101248. [CrossRef]

92. Zhou, Z.; Shen, H.; Liu, B.; Du, W.; Jin, J.; Lin, J. Residual thermal stress prediction for continuous tool-paths in wire-arc additive manufacturing: A three-level data-driven method. *Virtual Phys. Prototyp.* **2022**, *17*, 105–124. [CrossRef]

93. Abusalma, H.; Eisazadeh, H.; Hejripour, F.; Bunn, J.; Aidun, D.K. Parametric study of residual stress formation in Wire and Arc Additive Manufacturing. *J. Manuf. Process.* **2022**, *75*, 863–876. [CrossRef]

94. Tang, S.; Wang, G.; Huang, C.; Li, R.; Zhou, S.; Zhang, H. Investigation, modeling and optimization of abnormal areas of weld beads in wire and arc additive manufacturing. *Rapid Prototyp. J.* **2020**, *26*, 1183–1195. [CrossRef]

95. Raut, L.P.; Taiwade, R.V. Wire Arc Additive Manufacturing: A Comprehensive Review and Research Directions. *J. Mater. Eng. Perform.* **2021**, *30*, 4768–4791. [CrossRef]

96. Hejripour, F.; Valentine, D.T.; Aidun, D.K. Study of mass transport in cold wire deposition for Wire Arc Additive Manufacturing. *Int. J. Heat Mass Transf.* **2018**, *125*, 471–484. [CrossRef]

97. Vimal, K.E.K.; Naveen Srinivas, M.; Rajak, S. Wire arc additive manufacturing of aluminium alloys: A review. *Mater. Today Proc.* **2019**, *41*, 1139–1145. [CrossRef]

98. Zhang, J.; Wang, X.; Paddea, S.; Zhang, X. Fatigue crack propagation behaviour in wire+arc additive manufactured Ti-6Al-4V: Effects of microstructure and residual stress. *Mater. Des.* **2016**, *90*, 551–561. [CrossRef]

99. Derekar, K.S.; Addison, A.; Joshi, S.S.; Zhang, X.; Lawrence, J.; Xu, L.; Melton, G.; Griffiths, D. Effect of pulsed metal inert gas (pulsed-MIG) and cold metal transfer (CMT) techniques on hydrogen dissolution in wire arc additive manufacturing (WAAM) of aluminium. *Int. J. Adv. Manuf. Technol.* **2020**, *107*, 311–331. [CrossRef]

100. Derekar, K.S.; Ahmad, B.; Zhang, X.; Joshi, S.S.; Lawrence, J.; Xu, L.; Melton, G.; Addison, A. Effects of Process Variants on Residual Stresses in Wire Arc Additive Manufacturing of Aluminum Alloy 5183. *J. Manuf. Sci. Eng. Trans. ASME* **2022**, *144*, 1–13. [CrossRef]

101. Yildiz, A.S.; Koc, B.I.; Yilmaz, O. Thermal behavior determination for wire arc additive manufacturing process. *Procedia Manuf.* **2020**, *54*, 233–237. [CrossRef]

102. Pawlik, J.; Cieślik, J.; Bembenek, M.; Góral, T.; Kapayeva, S.; Kapkenova, M. On the Influence of Linear Energy/Heat Input Coefficient on Hardness and Weld Bead Geometry in Chromium-Rich Stringer GMAW Coatings. *Materials* **2022**, *15*, 6019. [CrossRef] [PubMed]

103. Shen, C.; Reid, M.; Liss, K.D.; Pan, Z.; Ma, Y.; Cuiuri, D.; <monospace> </monospace>Van Duin, S.; Li, H. Neutron diffraction residual stress determinations in Fe3Al based iron aluminide components fabricated using wire-arc additive manufacturing (WAAM). *Addit. Manuf.* **2019**, *29*, 100774. [CrossRef]

104. Rossini, N.S.; Dassisti, M.; Benyounis, K.Y.; Olabi, A.G. Methods of measuring residual stresses in components. *Mater. Des.* **2012**, *35*, 572–588. [CrossRef]

105. Carpenter, K.; Tabei, A. On residual stress development, prevention, and compensation in metal additive manufacturing. *Materials* **2020**, *13*, 255. [CrossRef]

106. Martina, F.; Roy, M.J.; Szost, B.A.; Terzi, S.; Colegrove, P.A.; Williams, S.W.; Withers, P.J.; Meyer, J.; Hofmann, M. Residual stress of as-deposited and rolled wire+arc additive manufacturing Ti–6Al–4V components. *Mater. Sci. Technol.* **2016**, *32*, 1439–1448. [CrossRef]

107. Liu, C.; Lin, C.; Wang, J.; Wang, J.; Yan, L.; Luo, Y.; Yang, M. Residual stress distributions in thick specimens excavated from a large circular wire+arc additive manufacturing mockup. *J. Manuf. Process.* **2020**, *56*, 474–481. [CrossRef]

108. Hönnige, J.R.; Colegrove, P.A.; Ahmad, B.; Fitzpatrick, M.E.; Ganguly, S.; Lee, T.L.; Williams, S.W. Residual stress and texture control in Ti-6Al-4V wire + arc additively manufactured intersections by stress relief and rolling. *Mater. Des.* **2018**, *150*, 193–205. [CrossRef]

109. Acevedo, R.; Sedlak, P.; Kolman, R.; Fredel, M. Residual stress analysis of additive manufacturing of metallic parts using ultrasonic waves: State of the art review. *J. Mater. Res. Technol.* **2020**, *9*, 9457–9477. [CrossRef]

110. Shaloo, M.; Schnall, M.; Klein, T.; Huber, N.; Reitinger, B. A Review of Non-Destructive Testing (NDT) Techniques for Defect Detection: Application to Fusion Welding and Future Wire Arc Additive Manufacturing Processes. *Materials* **2022**, *15*, 3697. [CrossRef]

111. Wang, X.; Wang, A. Finite element analysis of clamping form in wire and arc additive manufacturing. In Proceedings of the 7th International Conference on Modeling, Simulation, and Applied Optimization (ICMSAO), Sharjah, 4–6 April 2017; pp. 1–5.

112. Zhang, C.; Shen, C.; Hua, X.; Li, F.; Zhang, Y.; Zhu, Y. Influence of wire-arc additive manufacturing path planning strategy on the residual stress status in one single buildup layer. *Int. J. Adv. Manuf. Technol.* **2020**, *111*, 797–806. [CrossRef]

113. Jhavar, S. *Wire Arc Additive Manufacturing: Approaches and Future Prospects*; Woodhead Publishing: Sawston, UK, 2021.

114. Sun, R.; Li, L.; Zhu, Y.; Guo, W.; Peng, P.; Cong, B.; Sun, J.; Che, Z.; Li, B.; Guo, C. Microstructure, residual stress and tensile properties control of wire-arc additive manufactured 2319 aluminum alloy with laser shock peening. *J. Alloys Compd.* **2018**, *747*, 255–265. [CrossRef]

115. Hönnige, J.; Seow, C.E.; Ganguly, S.; Xu, X.; Cabeza, S.; Coules, H.; <monospace> </monospace>Williams, S. Study of residual stress and microstructural evolution in as-deposited and inter-pass rolled wire plus arc additively manufactured Inconel 718 alloy after ageing treatment. *Mater. Sci. Eng. A.* **2021**, *801*, 140368. [CrossRef]

116. Halisch, C.; Radel, T.; Tyralla, D.; Seefeld, T. Measuring the melt pool size in a wire arc additive manufacturing process using a high dynamic range two-colored pyrometric camera. *Weld. World* **2020**, *64*, 1349–1356. [CrossRef]

117. Shen, H.; Lin, J.; Zhou, Z.; Liu, B. Effect of induction heat treatment on residual stress distribution of components fabricated by wire arc additive manufacturing. *J. Manuf. Process.* **2022**, *75*, 331–345. [CrossRef]

118. Tanvir, A.N.M.; Ahsan, M.R.; Ji, C.; Hawkins, W.; Bates, B.; Kim, D.B. Heat treatment effects on Inconel 625 components fabricated by wire + arc additive manufacturing. *Int. J. Adv. Manuf. Technol.* **2019**, *103*, 3785–3798. [CrossRef]

119. Huang, J.; Li, Z.; Yu, S.; Yu, X.; Fan, D. Real-time observation and numerical simulation of the molten pool flow and mass transfer behavior during wire arc additive manufacturing. *Weld. World* **2022**, *66*, 481–494. [CrossRef]

120. Donoghue, J.; Antonysamy, A.A.; Martina, F.; Colegrove, P.A.; Williams, S.W.; Prangnell, P.B. The effectiveness of combining rolling deformation with Wire-Arc Additive Manufacture on β-grain refinement and texture modification in Ti-6Al-4V. *Mater. Charact.* **2016**, *114*, 103–114. [CrossRef]

121. Yang, Y.; Jin, X.; Liu, C.; Xiao, M.; Lu, J.; Fan, H.; Ma, S. Residual stress, mechanical properties, and grain morphology of Ti-6Al-4V alloy produced by ultrasonic impact treatment assisted wire and arc additive manufacturing. *Metals* **2018**, *8*, 934. [CrossRef]

122. Colegrove, P.A.; Coules, H.E.; Fairman, J.; Martina, F.; Kashoob, T.; Mamash, H.; Cozzolino, L.D. Microstructure and residual stress improvement in wire and arc additively manufactured parts through high-pressure rolling. *J. Mater. Process. Technol.* **2013**, *213*, 1782–1791. [CrossRef]

123. Li, R.; Xiong, J. Influence of interlayer dwell time on stress field of thin-walled components in WAAM via numerical simulation and experimental tests. *Rapid. Prototyp. J.* **2019**, *25*, 1433–1441. [CrossRef]

124. Montevecchi, F.; Venturini, G.; Grossi, N.; Scippa, A.; Campatelli, G. Heat accumulation prevention in Wire-Arc-Additive-Manufacturing using air jet impingement. *Manuf. Lett.* **2018**, *17*, 14–18. [CrossRef]

125. Nagamatsu, H.; Sasahara, H. Improvement of Cooling Effect and Dimensional Accuracy of Wire and Arc Additive Manufactured Magnesium Alloy by Active-Cooling-Based Contacting Copper Blocks. *J. Manuf. Mater. Process.* **2022**, *6*, 27. [CrossRef]

126. Maurya, A.K.; Yeom, J.T.; Kang, S.W.; Park, C.H.; Hong, J.K.; Reddy, N.S. Optimization of hybrid manufacturing process combining forging and wire-arc additive manufactured Ti-6Al-4V through hot deformation characterization. *J. Alloys Compd.* **2022**, *894*, 162453. [CrossRef]

127. Chi, J.; Cai, Z.; Wan, Z.; Zhang, H.; Chen, Z.; Li, L.; Li, Y.; Peng, P.; Guo, W. Effects of heat treatment combined with laser shock peening on wire and arc additive manufactured Ti17 titanium alloy: Microstructures, residual stress and mechanical properties. *Surf. Coatings Technol.* **2020**, *396*, 125908. [CrossRef]

128. Vazquez, L.; Rodriguez, M.N.; Rodriguez, I.; Alvarez, P. Influence of post-deposition heat treatments on the microstructure and tensile properties of ti-6al-4v parts manufactured by cmt-waam. *Metals* **2021**, *11*, 1161. [CrossRef]

129. da Silva, L.J.; Ferraresi, H.N.; Araújo, D.B.; Reis, R.P.; Scotti, A. Effect of thermal management approaches on geometry and productivity of thin-walled structures of er 5356 built by wire + arc additive manufacturing. *Coatings* **2021**, *11*, 1141. [CrossRef]

130. Ding, D.; Wu, B.; Pan, Z.; Qiu, Z.; Li, H. Wire arc additive manufacturing of Ti6AL4V using active interpass cooling. *Mater. Manuf. Process.* **2020**, *35*, 845–851. [CrossRef]

131. Vázquez, L.; Rodríguez, N.; Rodríguez, I.; Alberdi, E.; Álvarez, P. Influence of interpass cooling conditions on microstructure and tensile properties of Ti-6Al-4V parts manufactured by WAAM. *Weld. World* **2020**, *64*, 1377–1388. [CrossRef]

132. Wu, B.; Pan, Z.; Ding, D.; Cuiuri, D.; Li, H.; Fei, Z. The effects of forced interpass cooling on the material properties of wire arc additively manufactured Ti6Al4V alloy. *J. Mater. Process. Technol.* **2018**, *258*, 97–105. [CrossRef]

133. Geng, H.; Li, J.; Gao, J.; Lin, X. Theoretical model of residual stress and warpage for wire and arc additive manufacturing stiffened panels. *Metals* **2020**, *10*, 666. [CrossRef]

134. Graf, M.; Hälsig, A.; Höfer, K.; Awiszus, B.; Mayr, P. Thermo-mechanical modelling of wire-arc additive manufacturing (WAAM) of semi-finished products. *Metals* **2018**, *8*, 1009. [CrossRef]

135. Mishurova, T.; Sydow, B.; Thiede, T.; Sizova, I.; Ulbricht, A.; Bambach, M.; Bruno, G. Residual stress and microstructure of a Ti-6Al-4V wire arc additive manufacturing hybrid demonstrator. *Metals* **2020**, *10*, 701. [CrossRef]

136. Huang, W.; Wang, Q.; Ma, N.; Kitano, H. Distribution characteristics of residual stresses in typical wall and pipe components built by wire arc additive manufacturing. *J. Manuf. Process.* **2022**, *82*, 434–447. [CrossRef]

137. Khaled, H.; Abusalma, J. ODU Digital Commons Parametric Study of Residual Stresses in Wire and Arc Additive Manufactured Parts. Ph.D. Thesis, Old Dominion University, Norfolk, VA, USA, 2020.

138. Gordon, J.V.; Haden, C.V.; Nied, H.F.; Vinci, R.P.; Harlow, D.G. Fatigue crack growth anisotropy, texture and residual stress in austenitic steel made by wire and arc additive manufacturing. *Mater. Sci. Eng. A.* **2018**, *724*, 431–438. [CrossRef]

139. Heigel, J.C.; Michaleris, P.; Reutzel, E.W. Thermo-mechanical model development and validation of directed energy deposition additive manufacturing of Ti-6Al-4V. *Addit. Manuf.* **2015**, *5*, 9–19. [CrossRef]

140. Ahmad, B.; Zhang, X.; Guo, H.; Fitzpatrick, M.E.; Neto, L.M.S.C.; Williams, S. Influence of Deposition Strategies on Residual Stress in Wire + Arc Additive Manufactured Titanium Ti-6Al-4V. *Metals* **2022**, *12*, 253. [CrossRef]

141. Hoye, N.; Li, H.J.; Cuiuri, D.; Paradowska, A. Measurement of residual stresses in titanium aerospace components formed via additive manufacturing. *Mater. Sci. Forum* **2014**, *777*, 124–129. [CrossRef]

142. Ma, Y.; Hu, Z.; Tang, Y.; Ma, S.; Chu, Y.; Li, X.; Luo, W.; Guo, L.; Zeng, X.; Lu, Y. Laser opto-ultrasonic dual detection for simultaneous compositional, structural, and stress analyses for wire + arc additive manufacturing. *Addit. Manuf.* **2020**, *31*, 100956. [CrossRef]

143. Wu, Q.; Mukherjee, T.; Liu, C.; Lu, J.; DebRoy, T. Residual stresses and distortion in the patterned printing of titanium and nickel alloys. *Addit. Manuf.* **2019**, *29*, 100808. [CrossRef]

144. Zavdoveev, A.; Pozniakov, V.; Baudin, T.; Kim, H.S.; Klochkov, I.; Motrunich, S.; Heaton, M.; Aquier, P.; Rogante, M.; Denisenko, A.; et al. Optimization of the pulsed arc welding parameters for wire arc additive manufacturing in austenitic steel applications. *Int. J. Adv. Manuf. Technol.* **2022**, *119*, 5175–5193. [CrossRef]

145. Doumenc, G.; Couturier, L.; Courant, B.; Paillard, P.; Benoit, A.; Gautron, E.; Girault, B.; Pirling, T.; Cabeza, S.; Gloaguen, D.; et al. Investigation of microstructure, hardness and residual stresses of wire and arc additive manufactured 6061 aluminium alloy. *Materialia* **2022**, *25*, 101520. [CrossRef]

146. Hönnige, J.R.; Colegrove, P.A.; Ganguly, S.; Eimer, E.; Kabra, S.; Williams, S. Control of residual stress and distortion in aluminium wire + arc additive manufacture with rolling. *Addit. Manuf.* **2018**, *22*, 775–783. [CrossRef]

147. Li, K.; Klecka, M.A.; Chen, S.; Xiong, W. Wire-arc additive manufacturing and post-heat treatment optimization on microstructure and mechanical properties of Grade 91 steel. *Addit. Manuf.* **2021**, *37*, 101734. [CrossRef]

148. Cadiou, S.; Courtois, M.; Carin, M.; Berckmans, W.; Le Masson, P. 3D heat transfer, fluid flow and electromagnetic model for cold metal transfer wire arc additive manufacturing (Cmt-Waam). *Addit. Manuf.* **2020**, *36*, 101541. [CrossRef]

149. Kumar, M.D.B.; Manikandan, M. Evaluation of Microstructure, Residual Stress, and Mechanical Properties in Different Planes of Wire + Arc Additive Manufactured Nickel-Based Superalloy. *Met. Mater. Int.* **2022**, *28*, 3033–3056. [CrossRef]

150. Béraud, N.; Chergui, A.; Limousin, M.; Villeneuve, F.; Vignat, F. An indicator of porosity through simulation of melt pool volume in aluminum wire arc additive manufacturing. *Mech. Ind.* **2022**, *23*, 1–8. [CrossRef]

151. Manokruang, S. Phenomenological Model of Thermal Effects on Weld Beads Geometry Produced by Wire and Arc Additive Manufacturing (WAAM) Supasit Manokruang. Ph.D. Thesis, Université Grenoble Alpes, Gières, France, 2022.

152. Adebayo, A.; Ekiti, A. Characterisation of integrated WAAM and machining processes. Ph.D. Thesis, Cranfield University, Bedford, UK, 2013; p. 2020.